Submarine paleoseismology of the northern Hikurangi subduction margin of New Zealand as deduced from Turbidite record since 16 ka

Hugo Pouderoux, Jean-Noël Proust, Geoffroy Lamarche

SUBMARINE PALEOSEISMOLOGY OF THE NORTHERN HIKURANGI SUBDUCTION MARGIN OF NEW ZEALAND AS DEDUCED FROM TURBIDITE RECORD SINCE 16KA

Hugo Pouderoux[1,2,*], Jean-Noël Proust[1], Geoffroy Lamarche[2]

[1]Géosciences-Rennes, CNRS, Université Rennes1, Campus de Beaulieu, 35042, Rennes cedex, France. E-mail: h.pouderoux@gmail.com; jean-noel.proust@univ-rennes1.fr

[2]National Institute of Water and Atmospheric Research (NIWA), Private Bag 14-901, Wellington, 6241, New Zealand. E-mail: g.lamarche@niwa.co.nz

[*] Present day address: Department of Geoscience, University of Calgary, 2500 University Drive NW, Calgary, AB T2N 1N4, Canada

KEYWORDS

active margin; Poverty Bay; paleoearthquake; turbidite paleoseismology; synchronous slope failures; earthquake hazard assessment; peak ground acceleration

ABSTRACT

Paleoseismic studies seek to characterise the signature of pre-historical earthquakes by deriving quantitative information from the geological record such as the source, magnitude and recurrence of moderate to large earthquakes. In this study, we provide a ~16,000 yr-long paleo-earthquake record of the 200 km-long northern Hikurangi Margin, New Zealand, using cm-thick deep-sea turbidites identified in sediment cores. Cores were collected in strategic locations across the margin within three distinct morphological re-entrants – the Poverty, Ruatoria and Matakaoa re-entrants. The turbidite facies vary from muddy to sandy with evidence for rare hyperpycnites interbedded with hemipelagites and tephra. We use the Oxal probabilistic software to model the age of each turbidite, using the sedimentation rate of hemipelagite deduced from well-dated tephra layers and radiocarbon ages measurements on planktonic foraminifera.

Turbidites are correlated from one core to the other using similarity in sedimentary facies, petrophysical properties and ages. Results show that 46 turbidites are synchronous along the entire margin. Amongst them 41 are interpreted as originating from the upper continental slope in response to earthquake-triggered slope failures between 390 ±170 to 16,450 ±310 yr BP. Using well-established empirical relationships that combine peak ground acceleration, magnitude and location of earthquakes, we calculate that synchronous slope failures were triggered by the rupture of 3 of the 26 known active faults in the region, each capable of generating M_w 7.3 to 8.4 earthquakes – two are crustal reverse faults and one is the subduction interface. The 41 $M_w \geq 7.3$ earthquakes occurred at an average recurrence interval of ~400 yr over the last ~16,000 yr. Among them, twenty are interpreted as subduction interface earthquakes that occurred at a median recurrence interval of ~800 yr, with alternating periods of high activity and low return times (305 – 610 yr) and quiescence periods with high return times (1480 – 2650 yr). Based on turbidite paleoseismology, we propose that subduction interface earthquakes were of lower magnitude during active periods ($M_w > 7.5$) than during quiescence periods ($M_w \geq 8.2$).

1. INTRODUCTION

Submarine paleoseismology provides the means to derive reliable information on the spatial distribution and recurrence of prehistoric earthquakes in the marine environment from the

sedimentary record. The method has been successfully applied at active margins (Adams, 1990; Goldfinger et al., 2003; 2007; Huh et al., 2004; Noda et al., 2008; Gracia et al., 2010; McHugh et al., 2011), in lakes (Strasser et al., 2006; Beck, 2009), and in intraplate domains (St-Onge et al., 2004). However, identification of earthquakes as the triggering mechanism of turbidites often remains equivocal despite careful sedimentological characterization (e.g. Gorsline et al., 2000; Nakajima and Kanai, 2000). Convincing interpretations have been obtained by demonstrating a synchronicity of trigger over long distances and across distinct sedimentary systems (Goldfinger et al., 2003; 2007; Gracia et al., 2010). In some cases, correlations with historical and instrumental records of earthquakes substantiate the interpretations, but in regions where written history does not exceed 200 years like in New Zealand, specific methodologies need to be developed to ascertain the earthquake origin of turbidites (Pouderoux et al., 2012a; 2012b; Barnes et al., 2013).

The northern Hikurangi subduction margin, east of New Zealand's North Island contains well-developed series of Quaternary turbidites (Lewis, 1973, 1980; Lewis et al., 2004; Pouderoux et al., 2012a). It is characterised by high sediment delivery (Hicks and Shankar, 2003; Hicks et al., 2004), and intense tectonic activity (Reyners and McGinty, 1999; Doser and Webb, 2003), which makes it an excellent location for marine turbidite paleoseismology studies. Three large morphological re-entrants in the margin, the Poverty, Ruatoria and Matakaoa re-entrants (Fig. 1), concentrate gravity flow sedimentation (Lewis et al., 2004; Joanne et al., 2010; Pedley et al., 2010) and record a succession of turbidites emplaced since the Last Glacial Maximum (Pouderoux et al., 2012a). In Poverty re-entrant, Pouderoux et al. (2012b) demonstrated that most of the turbidites were triggered by paleo-earthquakes. However, their study focused on two cores recovered from a single sedimentary system and lacks the margin-scale embrace which may afford the characterisation of earthquakes of great magnitudes ($M_W > 8$) such as those generated along a subduction interface.

The present paper aims at establishing a calendar record of earthquakes that occurred along the northern Hikurangi Margin for the last ~16,000 yr, at identifying the fault sources and estimating the magnitude of earthquakes at the origin of the turbidites. To do so, we use sedimentological and geomoprhological observations, chronostratigraphic correlations and peak ground acceleration attenuation models.

2. BACKGROUND AND GEOLOGICAL SETTINGS

2.1. Morphological and tectonic settings

The northern Hikurangi Margin (Fig. 1) comprises from east to west the 3500 m-deep Hikurangi Trough, a narrow sediment-starved accretionary prism, an unstable continental slope and a continental shelf supplied in sediments by the rivers of the Raukumara Peninsula (Lewis, 1980; Lewis and Pettinga, 1993; Collot et al., 1996). The margin extends northwards into the Kermadec subduction margin. Inland, west of the peninsula lies the rhyolitic Central Volcanic Region, which is the main source of geochemically distinct ash layers (tephra) that punctuate the terrestrial and subaqueous Quaternary sedimentary record of the North Island (Lowe et al., 2008). Three morphological re-entrants scar the continental slope (Fig. 1): (1) the 1500 km^2 Poverty re-entrant which formed after successive margin collapses since 1500 ±500 ka (Pedley et al., 2010); (2) the 3300 km^2 Ruatoria re-entrant and associated Ruatoria Debris Avalanche formed 170 ±40 ka ago (Collot et al., 2001); and (3) the 1000 km^2 Matakaoa re-entrant located ~100 km landward of the subduction margin and resulting from multiple mass transport events deposited between 1300 and 35 ka (Lamarche et al., 2008a; Joanne et al., 2010). The three re-entrants (thereafter named Poverty, Ruatoria or Matakaoa for simplicity) include gullies and canyons on the upper slope, mid-slope basins and trench basins, and represent independent Quaternary sedimentary systems.

The subduction of the Pacific Plate beneath the Australian Plate, at a present rate of 5 cm/yr (DeMets et al., 1994; Beavan et al., 2002) is resulting in uplifting of the inland axial range of the

Raukumara Peninsula at an estimated maximum rate of 3 mm/yr (Reyners and McGinty, 1999; Wilson et al., 2007), and intense seismic activity along the margin (e.g. Webb and Anderson, 1998; Reyners and McGinty, 1999). Quantitative estimate of the interseismic coupling (Wallace et al., 2004; 2009), seismological studies (Reyners, 1993; 1998), tectonic investigations (Nicol and Wallace, 2009) and geomorphological characteristics (Collot et al., 1996) all contribute to the interpretation that the 600 km-long Hikurangi Margin divides into three subduction interface segments, namely from south to north, the Wairarapa, Hawke's Bay and Raukumara segments. The change from accretion to erosion-dominated margin, North of Gisborne marks the transition from Hawke's Bay to Raukumara segments, where the study area is located. Empirical modelling suggests that rupture of the Raukumara or Hawke's Bay segment would result in M_w 8.2 – 8.4 earthquakes, whereas a simultaneous rupture of both segments would produce a M_w 8.6 earthquake, and that rupture of the entire Hikurangi Margin would result in a M_w 8.8 earthquake (Wallace et al., 2009; Stirling et al., 2012). Northwards, the Kermadec Margin may trigger $M_w \geq 8.5$ earthquakes that can affect the study area (Power et al., 2011). Seismic reflection surveys on the continental shelf have helped to identify a series of upper plate active faults (Barnes et al., 2002; Barnes and Nicol, 2004; Lewis et al., 2004; Fig. 1) and empirical relationships suggest some of these faults are capable of generating $M_w \geq 6.5$ earthquakes (Stirling et al., 2012; see also SM1).

The instrumental record of earthquakes in New Zealand since 1940 includes 298 earthquakes of $M_w > 5$ in the study area, with only six of $M_w \geq 6.5$ (*http://www.geonet.co.nz*, as in December 2011). Two subduction interface earthquakes of M_w 6.9 – 7.1 were recorded in 1947 in the Poverty Bay area (Downes et al., 2000; Doser and Webb, 2003), and the 1931 M_w 7.8 Napier upper plate earthquake is the largest and most damaging historic earthquake recorded in the area (Downes, 1995). Prehistoric $M_w \geq 7$ earthquakes over the last 9 kyr are evidenced by uplifted marine terraces (Berryman, 1993; Wilson et al., 2006; 2007), subsided swamps (Cochran et al., 2006) and tsunami deposits (Goff and Dominey-Howes, 2009). Marine terraces uplifts at Pakarae river mouth and Mahia Peninsula are thought to be the result of near-shore fault ruptures (Wilson et al., 2007; Litchfield et al., 2010), namely the Gable End and Lachlan 3 faults (Fig. 1), that might have ruptured coevally. Sudden subsidence episodes at the origin of swamps flooding in Hawke's Bay were interpreted as the result of large offshore earthquakes either from ruptures of the Lachlan 3 fault or the subduction interface (Fig 1; Cochran et al., 2006). In Poverty, a 18 kyr paleo-earthquake record based on turbidite deposition reveal a mean return time of ~230 years for moderate to large earthquakes and a 90% probability of occurrence ranging from 10 to 570 years (Pouderoux et al., 2012b). Probabilistic seismic hazard assessment suggests that earthquakes in the region with an associated Peak Ground Acceleration (PGA) of 0.3-0.5 g have a 500-year return time in the coastal area and that earthquakes with a PGA of 0.8-1.4 g have a 2500 year average return time (Stirling et al., 2012).

2.2. Sedimentation patterns and turbidites deposition

The ubiquitous gravity flow sedimentation of the northern Hikurangi Margin ranges from fine turbidites deposited on mid-slope basins to margin-scale debris avalanches (Lewis, 1973; Collot et al., 2001; Lamarche et al., 2008a; Mountjoy and Micallef, 2011; Pouderoux et al., 2012a). Quaternary sedimentation is characterised by interlayering of turbidites and hemipelagites infilling slope and trench basins (Lewis, 1980; Lewis and Pettinga, 1993; Lamarche et al., 2008b; Paquet et al., 2011). Over the last ~18 kyr, accumulation rates in mid-slope basins and in the Hikurangi Trough range from ~15 to ~110 cm/ka (Orpin, 2004; Orpin et al., 2006; Pouderoux et al., 2012a). The Waipaoa and Waiapu rivers (Fig. 1) provide most of the turbidite material, contributing to an annual sediment delivery of 70 Mt/yr off the Raukumara Peninsula (Hicks and Shankar, 2003). The present day sedimentation rate estimated from ^{210}Pb activity decreases from ~1,000 cm/ka on the continental shelf to ~100 cm/ka in mid-slope basins (Alexander et al., 2010; Kniskern et al., 2010), but forest clearing during human settlement in New Zealand 500 – 700 yr ago resulted in river sediment fluxes

110 to 660% greater than during the Holocene interglacial period (McGlone and Wilmshurst, 1999; Kettner et al., 2007; Paquet et al., 2009).

Turbidites along the northern Hikurangi Margin are recognised as cm-thick fining up sandy to silty beds rich in volcaniclastic debris, quartz and bioclasts (Pouderoux et al., 2012a; Fig. 2). Few debrites, characterised by <35 cm-thick chaotic silty-clay beds with sand to pebble size clasts are also recognised. These two lithotypes alternate with hemipelagites, which consists of 1 – 90 cm-thick layers of olive-grey silty-clay, and tephra layers, composed of volcaniclastic debris, mainly glass shards and pumiceous lapilli, and arranged in <10 cm-thick silty beds (Table 1). Boundaries between lithotypes are usually sharp, except between turbidites tails and hemipelagites.

Turbidites tails and hemipelagites have similar grain-size and texture but differ by their colours, with hemipelagites being lighter than turbidites. Hemipelagites are better sorted than turbidites, with a characteristic single grain-size peak < 10 µm. The composition of the silty fraction in hemipelagites explains the colour variations with abundant volcaniclastic debris and low quartz content when compared to turbidites, which show abundant quartz and low volcaniclastic debris. The differences are confirmed by $\delta^{13}C$ and C/N values, with higher $\delta^{13}C$ and lower C/N in hemipelagites than in turbidites (Pouderoux et al., 2012b). Erosion at the base of turbidites is considered negligible for those deposited during the Holocene but common during the Late Pleistocene (Pouderoux et al., 2012a). Floods and volcanic eruptions may have occasionally triggered turbidity currents in the area and resulted in the deposition of hyperyncites and primary monomagmatic turbidites (Pouderoux et al., 2012a). The majority of turbidites contains benthic foraminifers indicative of environments ≥150 m, suggesting an upper slope origin of the reworked material. In Poverty, 67 synchronous turbidites are interpreted as being originated from earthquake-triggered slope failures on the upper continental slope between 820±190 and 17,730±700 yr BP (Pouderoux et al., 2012b).

3. METHODS

3.1. Sediment core analyses

The present study is based on detailed stratigraphic correlation of sediment cores collected in Poverty, Ruatoria and Matakaoa (Fig. 1; Table 2). Cores were recovered from strategic locations to sample turbidites deposition since the Last Glacial Maximum (Proust et al., 2006). Four giant piston cores, 12 to 20 m long, were collected during the MD152 MATACORE voyage of *R.V. Marion-Dufresne* (Proust et al., 2006; 2008) in Poverty and Ruatoria in water depth ranging from 1400 to 3500 m. In Poverty, MD06-3003 and MD06-3002 targeted two mid-slope basins in water depths of 1390 m and 2300 m respectively. In Ruatoria, MD06-3009 was collected in 2940 m water depth on top of the Ruatoria Debris Avalanche and ~250 m above main sediment pathways. MD06-3008 was collected in 3520 m water depth in the Hikurangi Trough. Nine short piston cores were acquired onboard *R.V. Tangaroa* during research voyages TAN0314 (Carter et al., 2003) and TAN0810 (Lamarche et al., 2008b) in Ruatoria and Matakaoa in water depth ranging from 650 to 3400 m. In Ruatoria, Tan0810-2 and -3 were collected on the upper continental slope in water depth of ca. 1080 m, and Tan0810-6 was retrieved from the floor of the 3400 m-deep Hikurangi Trough. In Matakaoa, Tan0810-9 to -13 were collected within the channel/levee complex of the Matakaoa Turbidite System in water depth ranging from 1090 to 1260 m (Fig. 1). More specifically, Tan0810-9 and -12 were collected within the Matakaoa channel, Tan0810-10 on the left hand levee and Tan0810-11 and -13 on the right hand levee, all less than 2 km away from the channel. Tan0314-8 was collected within the deep-sea fan in 2030 m water depth.

Petrophysical analyses, including continuous gamma density, magnetic susceptibility and P-wave velocity, were obtained on split cores at 1 cm intervals using a Geotek Multi-Sensor Track. These measurements tied to the main lithofacies and lithofacies successions proved to be essential for core-to-core correlation. P-wave velocities tends to be underestimated (1200-1500 m/s) but the

downcore fluctuations, which were used for core-to-core correlations are similar to those in the density and magnetic susceptibility measurements as well as facies variations so that they are considered usable.

3.2. Age model

The stratigraphic framework is based on tephrochronology and AMS ^{14}C radiochronology with an average frequency of 0.7 to 2 ages per meter of core (Pouderoux et al., 2012a). Tephra were characterised by glass chemistry, mineralogy and their stratigraphic position and tied to the well-established regional charts of volcanic eruptions to get their precise calibrated ages (Shane, 2000; Lowe et al., 2008). The cores contain one to six tephra layers correlated to the nine large volcanic eruptions that occurred in the Central Volcanic Region. Radiocarbon dating was performed on hand-picked mixed planktonic foraminifers from hemipelagite samples collected 0.7-1.0 cm below turbidite layers. Raw radiocarbon ages are calibrated using the Oxcal 4.1 software (Bronk Ramsey, 2008) with a regional reservoir age of 395 ±57yr (ΔR= -5 ±57yr) calculated from the published East Cape reservoir ages (Kalish, 1993; Higham and Hogg, 1995). A reservoir age of 800 ±110 yr (ΔR= 400 ±110yr) was applied for ^{14}C dates between 12,400 and 12,900 ^{14}C yr BP, as temporal variations of the reservoir age were identified during this period (Carter et al., 2008; Sikes et al., 2000).

We derive the age model for each core by interpolating hemipelagite sedimentation rates between time markers (tephra and ^{14}C ages) according to the *P_Sequence* deposition model of the Oxcal 4.1 software, following the approach developed by Pouderoux et al. (2012b). The model provides the 68% and 95% probability age ranges (1σ and 2σ) of each turbidite. In the following sections, ages are reported with 2σ uncertainties. The 2σ ages are considered reliable for Holocene turbidites as basal erosion is negligible, but the age may be overestimated during the Late Pleistocene when basal erosion is likely to have occurred (Pouderoux et al., 2012a).

3.3. Correlation criteria

We use four criteria to correlate turbidites from core to core (see SM2). (1) Tephra layers form absolute time-lines and robust stratigraphic markers. Their identification in distinct cores constitutes the first criteria for correlating events across the margin. (2) The estimated age of each turbidite is used as second criteria to make stratigraphic correlations between two tephra layers. However, because of the high number of turbidites and their age uncertainties, correlation from on core to another can be ambiguous at time. (3) We use the similarity in petrophysical properties (gamma density, magnetic susceptibility and P-wave velocity) and facies as third criteria, and (4) the thickness of turbidites and hemipelagite as fourth criteria to ascertain the correlations. Petrophysical properties are good correlation criteria (Patton et al., 2013; Goldfinger et al., 2012; Gracia et al., 2010) because turbidite coarse grain-size or volcaniclastic compositions typically result in high densities, magnetic susceptibilities and P-wave velocities and correlate well from core to core (Fig. 2).

3.4. Terminology

In this study, the term "*turbidite event*" (Tx) refers to a single, well-dated depositional episode under- and overlain by hemipelagite. Stacked turbidites with no intertwined hemipelagite are considered as a single depositional event, as only the presence of hemipelagite guarantees the occurrence of significant time between two successive events. Two turbidites separated by a tephra layer represent two distinct events as usually tephra settle down within days to months after the volcanic eruptions (Wiesner et al., 1995).

"*Basin events"* represent synchronous turbidite events recorded in at least two cores in a single re-entrant. Basin events are labelled *Px* in Poverty, *Rx* in Ruatoria and *Mx* in Matakaoa, *x* being the event sequential number in the re-entrant from the youngest to the oldest.

Hikurangi "*margin events" (Hx)* are synchronous *basin events* recorded in at least two re-entrants along the northern Hikurangi Margin. The age of a *margin event* is determined by the intersection of the age ranges shared by the synchronous *basin events*. Non-correlative events are called "*isolated events"*.

4. RESULTS

4.1. Petrophysical properties of sediments

The downcore variability in gamma density, magnetic susceptibility (MS) and P-wave velocity (V_p) depends on sediment lithology and the alternation of hemipelagites, turbidites and tephra (Fig. 2; Table 3). Hemipelagites usually have constant low density (1.1 to 1.8 g/cm^2), MS (10 to 60 SI) and V_p (1225 to 1775 m/s). Turbidites have systematically higher density (1.2 to 2.2 g/cm^2), MS (10 to 120 SI) and V_p (1225 to 1950 m/s) with a decreasing trend from base to top. When preserved, tephra show values similar to turbidites, but higher than hemipelagites, with characteristic sharp variations at their base and top boundaries.

The boundary between turbidites and hemipelagites is progressive and difficult to identify using petrophysical properties alone. Turbidites show generally a progressive decrease while hemipelagites have stable values. Usually the decreasing trend of turbidite sequence is in good agreement with grain-size measurements, and coarser beds are noticed by a sharp increase of the density, MS and V_p (Fig. 2).

4.2. Age model and time-lines

Cores in Ruatoria cover a continuous age range from 630 ±10 yr BP to 15,360 ±70 ^{14}C yr, with the oldest sediments contained in cores MD06-3008 and MD06-3009 (Pouderoux et al., 2012a). In Matakaoa, cores from the turbidite plain (Tan0810-9 to -13) cover a continuous age range from 630 ±10 yr BP to 4,710 ±40 ^{14}C yr. In core Tan0314-8, two basal ^{14}C ages complement the tephra identification of Joanne et al. (2010), and show that the core contains a truncated record from 5,530 ±60 yr BP to 13,910 ±70 ^{14}C year.

Age models provide an age estimate for every single turbidite event (Fig. 3). Overall the average 2σ age range is 410 years (13 – 1141) in Ruatoria and 327 years (13 – 970) in Matakaoa, comparable to the 300 year (25 – 757) 2σ age range calculated in Poverty (Pouderoux et al., 2012b). The ages of turbidite events in Ruatoria and Matakaoa correspond to the ages calculated at each corrected depth and ranges from 170 ±140 to 18,150 ±150 yr BP, similar to what was determined in Poverty (820 ±190 to 17,730 ±700 yr BP). From 0 to 6 kyr, 11 cores (all but MD06-3002 and Tan0314-8) are usable to correlate turbidite events along the margin, while from 6 to 17 kyr, only five cores provide potential for turbidite events correlations.

4.3. Core-to-core correlations

4.3.1. *At basin scale*

In Ruatoria, turbidite events are thick, commonly >10cm, and correlate well from the upper slope to the top of the debris avalanche and the Hikurangi Trough (Fig. 4; see also SM2 Fig. SM2.01). Cores on the upper slope (Tan0810-2 and -3) and on the top of the Ruatoria Debris Avalanche (MD06-3009) contain only basin events whereas the cores in the Hikurangi Trough (MD06-3008 and Tan0810-6) contain basin events and scattered isolated events. Two of these isolated events are primary monomagmatic turbidites deposited directly after the Taupo and Waimihia eruptions (Pouderoux et al., 2012a). We identified 30 basin events in Ruatoria, from 390 ±250 to 15,940 ±580yr BP. Basin events younger than 6 ka (R1 to R14) correlate in all five cores, whereas events from 6 to 17 ka (R15 to R30) correlate only in cores MD06-3008 and MD06-3009 (R15 to R30). The mean recurrence

intervals of these 30 basin events is 520 years. Only MD06-3009 contains material older than ~17 ka with a recurrence intervals of turbidite events of 97 years. This important difference in return time suggests that these turbidite events cannot be used as proxy for basin events for the period older than ~17 kyr.

In Matakaoa, turbidite events are commonly <5cm-thick, and often homogenised in the hemipelagite background because of severe bioturbation, hence a higher uncertainty in our interpretion of thin events as isolated or basin events than for Ruatoria and Poverty. We identify 19 basin events (M1 to M19) deposited in Matakaoa between 170±140 and 16,400±780 yr BP (Fig. 5; see also SM2 Fig. SM2.02). Basin events younger than 5 ka are only recognised in the turbidite plain (M1 to M9). Cores Tan0810-9, -10 and -13 mostly record basin events while cores Tan0810-11 and -12 are scattered with isolated events. Basin event M10 dated at 5,130±290 yr BP is the only event that correlates in the turbidite plain (Tan0810-10) and the deep-sea fan (Tan0314-8). No other events in the deep-sea fan correlate with upslope events because of the lack of age overlap in cores. Although this characterises them as isolated events, they likely represent basin events as the core was collected in the deep-sea fan at the outlet of the Matakaoa Turbidite System.

4.3.2. *At margin-scale*

Twenty-eight basin events are synchronous in two or more re-entrants over the last ~16 kyr, and therefore fulfil the criteria of margin events (Fig. 6; see also SM2 Fig. SM2.03). Ten margin events are documented in the three re-entrants (H3, H5, H8, H12, H23, H30, H33, H35, H41, and H43; Table 4). H4 and H6 are identified from correlative basin events in Poverty and Ruatoria but also correlate to isolated events in Matakaoa. The remaining 16 margin events are only correlative in Poverty and Ruatoria (H7, H9-11, H13-14, H16, H18-19, H22, H26-28, H31-32, and H34; Table 4). All basin events in Ruatoria, except for the two youngest R1 and R2 dated at 390 ±250 and 790 ±200 yr BP, fulfil the criteria of margin events. Originally, R1 and R2 were not recognised as margin events since they did not correlate to basin events in Poverty. However, because R1 and R2 correlate to isolated events in Matakaoa and because material younger than 820 yr BP was not retrieved in Poverty cores, we interpret them as margin events as all basin events in Ruatoria are margin events (H1 and H2 in Table 4).

A further 15 basin events in Poverty, dated from 6 to 16 kyr (P24, P26, P30, P33, P38, P40, P49, P57-61, P63, P65 and P66), correlate to 16 isolated events in core MD06-3008, and are interpreted as margin events (H15, H17, H20, H21, H24, H25, H29, H36-40, H42 and H44-46; Table 4). That specific period recorded in Ruatoria only by cores MD06-3008 and MD06-3009 is characterised by an unknown number of MD06-3008 isolated events not recognised as Ruatoria basin events due to a lack of data, as core MD06-3009 is located on a topographic high. In addition, during the period 0-6 kyr recorded in all cores, seven basin events not recorded in MD06-3009 (R1-2, R8-9, R11-12 and R14) fulfil the criteria of margin events. These observations confirm that the 15 correlated basin events in Poverty with isolated events in MD06-3008 are margin events.

Overall, the margin-scale correlation results in the identification of 46 margin events deposited from 390 ±170 to 16,450 ±310 yr BP, with an average age uncertainty of ~170 years (ranging from 6 to 400 years; Table 4).

5. DISCUSSION

5.1. Earthquake's origin of turbidites

The associations of benthic foraminifers contained in basin and isolated events suggest a shelf edge origin of the reworked material within 150-200 m of water depth in Ruatoria and Poverty, and 150-600 m of water depth in Matakaoa (Pouderoux et al., 2012a; 2012b). Isolated events in the trench interpreted as margin events also rework material from the upper slope, which corroborates that

turbidity currents originate from the upper slope and suggests a slope failure origin of most gravity flows. This suggestion is supported by the present day high state of instability of the Hikurangi Margin's upper slope associated with gas and fluids (Lewis and Marshall, 1996; Orpin, 2004; Faure et al., 2006), and high sediment supply during the Holocene (Hicks and Shankar, 2003; Addington et al., 2007; Lewis et al., 2004). At margin-scale, five margin events are interpreted as triggered by mechanisms other than slope failure: H9, H22, H23 and H28 which contain at least one hyperpycnite, and H5 which is a primary monomagmatic turbidite. The remaining 41 margin events are related to synchronous slope failures along the 100 km-long northern Hikurangi Margin and all originated within 150-600 m of water depth since ~16ka (Table 4; see also SM2 Fig. SM2.03).

Synchronicity of trigger over such wide areas is recognised as the most likely signature of large earthquakes in other regions of the world (Gracia et al., 2010; Goldfinger et al., 2003; 2012), although storms and tsunami waves may occasionally trigger gravity flows and slope failures (Mulder et al., 2001; Puig et al., 2004). Repeated storms have occurred along the northern Hikurangi Margin over the Late Holocene (Page et al., 2010), and are likely to have affected the seafloor by remobilising surficial sediments of the shelf or to have triggered sediment liquefaction (Lee and Edwards, 1986; Ma et al., 2010; Goldfinger et al., 2012). Puig et al. (2004) characterized sediment gravity flows directed down-canyon during storms on the California margin, and Mulder et al. (2001) described a storm-generated turbidite at 650 m water depth in a canyon head few months after a large historical storm in the Bay of Biscay. Furthermore, turbidity currents generated during storms are typically less voluminous and spread over smaller geographic areas than those triggered by earthquakes (Gorsline et al., 2000; Goldfinger et al., 2007; Blumberg et al., 2008). They also usually settle in water depth < 1000 m (Puig et al., 2004). The Matakaoa canyon's head contains a stack of recent cm-thick turbidites recorded in 650 m water depth, sedimentologically similar to the storm-induced turbidites found in the Bay of Biscay (Pouderoux, 2012; Pouderoux et al., 2012a). Even if confirmed along the Hikurangi Margin, these storm-related turbidites are likely to be restricted to canyon heads and not observed at water depth > 1000 m where we found deep-sea synchronous turbidites. Tsunami waves may also generate slope failures or turbidity currents directed down-slope and initiated on the continental shelf (Shanmugam, 2006). The largest historical tsunami affecting the region produced a run-up of ~10 m north of Gisborne and was triggered by the local M_w 7.1 Gisborne earthquake of 25 March 1947 (Downes et al., 2000; Doser and Webb, 2003). Other tsunami run-ups of 10 m interpreted as likely generated by local earthquakes appear in the New Zealand paleo-tsunamis record (Goff and Dominey-Howes, 2009). The tsunami generated by the 23 May 1960 M_w 9.5 Chilean earthquake, the largest earthquake ever recorded worldwide, resulted in a 3 m-high run-up at Gisborne and 4.5 m in Hawke's Bay (*geonet.org.nz*). This suggests that tsunamis potentially able to trigger slope failures are more likely to be generated by local earthquakes, which ground-shaking is far more likely to trigger slope failures than the tsunamis wave itself.

Earthquakes are therefore the most likely triggering mechanism during the last sea-level highstand for the generation of synchronous slope failures at the origin of margin events, as inferred in other active margins (e.g. Noda et al., 2008; Gracia et al., 2010; Goldfinger et al., 2012). Storms and tsunamis are possibly secondary players during the marine trangression. Even if the average recurrence interval of margin events varies slightly between the Late Holocene highstand (~440 yr over the last 7.5 kyr) and the Late Pleistocene – Early Holocene marine transgression (~375 yr from 7.5 to 16ka), it is possible that earthquake ground shaking was not the sole triggering mechanism of synchronous slope failures before 7.5 ka. It is extremely difficult to estimate the impact of storms and tsunamis waves on slope stability during the marine transgression. Consequently, if the turbidite record of the northern Hikurangi Margin is considered a good proxy for paleo-earthquakes during the Late Holocene and provides a calendar of 17 large earthquakes that occurred in the region between 390 ±170 and 7480 ±120 yr BP with an average return time of ~440 years, the Late Pleistocene – Early Holocene part of this record incurs an increased uncertainty. Nevertheless, the turbidite record during the marine transgression could be use complementary to the Late Holocene highstand to

constraint the earthquake hazard on the area, knowing that the recurrence intervals may be underestimated and the hazard overestimated.

5.2. Source and magnitude estimation of paleo-earthquakes

The 9 kyr-long coastal paleo-earthquake record is time correlative to margin events (Fig. 7). The 2σ age range of margin events overlies the age of all marine terraces uplifts except one at Pakarae river mouth and one at Mahia peninsula. These uplifts were interpreted as the result of the rupture of near-shore Gable End and Lachlan 3 faults (Wilson et al., 2007; Litchfield et al., 2010). Conclusions are however sometimes equivocal: H4 and H10 are time correlative to the rupture of these two faults suggesting a simultaneous rupture of the two faults or a rupture of the subduction interface; H1 correlates with uplifts at the Pakarae river mouth and Mahia Peninsula and with a paleo-tsunami.

Over the last 7.5 kyr, ten margin events correlate to the paleo-earthquake record onland. These margin events are part of a group of 20 particularly large margin events identified over the last 16 ka (Table 4; see also SM2 Fig. SM2.03), characterized by a ~40 cm-thick turbidite layer deposited on a topographic high in Ruatoria, ~250 m above the main sediment pathways (core MD06-3009); such thickness is twice that of turbidites in other cores. They correspond to exceptionally voluminous turbidity currents triggered simultaneously in the three re-entrants. Such sedimentological evidences coupled with the systematic correlation with onland record are consistent with a triggering by subduction earthquakes initiated on the Raukumara segment of the subduction interface.

Slope failure triggering and turbidite deposition depend more on the shaking intensity felt on the slope than on the magnitude of the earthquake itself. The shaking intensity can be evaluated by calculating the peak ground acceleration (PGA) (Lee and Edwards, 1986; Douglas, 2000). The PGA threshold for slope failure and turbidity current generation in conditions similar to the upper slope of the northern Hikurangi Margin ranges from 0.08 to 0.6 g and more likely from 0.08 to 0.15 g (Lee et al., 1999; Lykousis et al., 2002; Strasser et al., 2007; Noda et al., 2008; Dan et al., 2009; see also SM3). By using the PGA empirical attenuation relationships of Cousins et al. (1999) and Si and Midoriwaka (1999), which are best suited for the region, we estimated the earthquake magnitude (M_w) and the location of the hypocentre (depth and distance from the upper slope) of paleoearthquakes responsible for the triggering of upper slope failures. This enabled us to create isomagnitude maps and to identify areas where an earthquake of a given magnitude and origin has to occur to trigger synchronous slope failures and turbidity currents (Fig. 8; see also SM3 Fig. SM3). Superposing these isomagnitude maps over the known active faults (Stirling et al., 2012; Litchfield et al., in press) provides the means to infer the sources of paleo-earthquakes capable of generating our deep-sea turbidite record. (Table 5; see also SM3 Fig. SM3).

We disregard using a PGA threshold of 0.15 g for the triggering of turbidity currents as this would suggests that the 17 Late Holocene margin events were all subduction interface earthquakes, which is very unlikely (Table 5). A more reasonable PGA threshold between 0.08 and 0.1 g suggests that these events were associated with ruptures of upper plate faults or the subduction interface, all capable of generating $M_w \geq 7.3$. This latter interpretation is more consistent with our findings that only 10 out of these 17 margin events correspond to large subduction interface earthquakes. These values of PGA are also extremely closed to that determined along the Japan (Noda et al., 2008) and Algerian margins (Dan et al., 2009).

The 17 margin events provide a meaningful calendar of $M_w \geq 7.3$ paleo-earthquakes that have affected the region between 390 ±170 and 7,480 ±120 yr BP : 10 subduction interface earthquakes and 7 upper plate earthquakes (Tables 4 and 5). The results show that only three out of the 26 known active fault sources recognized by Stirling et al. (2012) in the offshore northern Hikurangi Margin (faults 2, 6 and 7, namely the Raukumara subduction interface segment, Ruatoria South 1 and Areil Bank; Table 5) are responsible for this deep sea turbidite record.

5.3. Recurrence intervals of large earthquakes

Our turbidite paleoseismology approach reveals that the recurrence interval (RI) of $M_w \geq 7.3$ earthquakes ranges from 150 to 1240 years with an average of 440 years during the Late Holocene (Figs. 9 and 10). Seismological modelling shows that the three active faults identified as the potential sources of our paleo-earthquakes have an empirical RI of rupture of 1300-1670, 3340, and 720 years (Table 5; see also SM1; Stirling et al., 2012). Assuming that upper plate faults rupture independently from the subduction interface (Stirling et al., 2012), the average RI of fault ruptures would be comprised between 390 and 460 years, which fits well with the 440 years RI of margin events. During the Late Pleistocene – Early Holocene, margin events had an average RI of 350 years, ranging from a few years to up to 1100 years, which is in good agreement with the estimated average RI of fault ruptures from Stirling et al. (2012).

The RI of the 10 large margin events triggered by subduction interface earthquakes varies from 370 to 2090 years during the Late Holocene with alternating periods of high and low RI, and an average RI of ~800 years. A similar pattern is recorded for the Late Pleistocene – Early Holocene period. Assuming that subduction interface earthquakes are the sole triggering mechanism of these large margin events over the last 16 kyr, this pattern of RI suggests two different tectonic regimes with periods of intense activity separated by periods of relative quiescence (Fig. 9). Such scenarios have been suggested by Berryman et al. (1989) for the Hikurangi Margin, Patton et al. (2009) for the Sumatra margin and Goldfinger et al. (2009; 2013) for the Cascadia margin. Active periods exhibit shorter durations (0.6-3 kyr-long) and drastically shorter RI (305-610 years) than quiescence ones (1.5-3.2 kyr-long with RI range of 1480-2650 years). These RIs differ from the predicted 1300-1670 years calculated using seismological modelling by Stirling et al. (2012). The latter RIs are closer to that observed during periods of quiescence than that during active periods. The RI and M_w of Stirling et al. (2012) are maximum values determined from empirical relationships and represent the time needed for the subduction interface to accumulate enough strain to rupture the full length of the Raukumara segment. Active seismic periods recorded in the sedimentary record suggest that in a stable tectonic regime (convergence rate, slip rate, etc…), the deformation and energy released by the subduction interface may be partitioned with multiple ruptures generating earthquakes less that M_w 8.2 – 8.4.

Isomagnitude maps suggest that a M_w 7.5 – 8 earthquake on the subduction interface segment would be enough to generate a PGA of 0.08 – 0.1 g on the upper slope and therefore trigger simultaneous turbidity currents along the northern Hikurangi Margin (see SM3 Fig. SM3). Considering the constraint given by core MD06-3009 and the presence of turbidites on topographic highs, we propose that during active periods the Raukumara segment of the subduction interface produced regular large M_w 7.5 – 8 earthquakes. These earthquakes may not rupture the full length of the Raukumara segment or release the total accumulated strain. This is in good agreement with the two inferred moderate subduction interface earthquake Mw 7 and 7.1 which affected the Gisborne district in 1947 (Doser and Webb, 2003).

6. CONCLUSION

This study presents the first chrono-stratigraphic correlation of deep-sea turbidites along the northern Hikurangi Margin of New Zealand, from the detailed description and age dating of sixteen sediment cores collected in the Poverty, Ruatoria and Matakaoa re-entrants. Age models provide a precise age estimate for every single turbidite deposited since the Last Glacial Maximum. The age of turbidites ranges from 170 ±140 to 18,150 ±150 yr BP.

Basin-scale correlations of turbidites result in the identification of 30 basin events (synchronous turbidites) deposited in Ruatoria between 390 ±250 and 15,940 ±580yr BP, and 19 basin events deposited in Matakaoa between 170 ±140 and 16,400 ±780 yr BP. Previous studies have recognised 73 basin events in Poverty, deposited between 820 ±190 and 17,730 ±700 yr BP.

Margin-scale correlations result in the identification of 46 margin events (synchronous basin events) deposited from 390 ±170 to 16,450 ±310 yr BP, among which four are recognised as catastrophic floods deposits (hyperpycnites) and one a primary monomagmatic turbidite. The remaining 41 margin events are related to synchronous slope failures along the margin.

Earthquakes are the triggering mechanism of these slope failures during the sea-level highstand, and are also likely to be the main triggering mechanism during the marine transgression. The turbidite record of the northern Hikurangi Margin is therefore a good proxy for paleo-earthquakes, corroborated by the time correlation with onland paleo-earthquake evidences.

The use of empirical relationships evaluating the upper slope stability allows us to estimate magnitude M_w and location (depth and distance from the upper slope) of paleo-earthquake. The 41 margin events correspond to $M_w \geq 7.3$ earthquakes that have affected the region from 390 ±170 to 16,450 ±310 yr BP, involving 3 of the 26 known active faults in the region (10%). Recurrence interval deduced from turbidite chronology is similar to the estimated activity of these three active faults. Twenty margin events are interpreted as subduction interface earthquakes of $M_w > 7.5$ and up to 8.4 affecting the three re-entrants and able to trigger coeval voluminous turbidity currents together with onland paleoseismic evidences.

Our study shows that large earthquake of $M_w \geq 7.3$ occurring on the northern Hikurangi Margin are more likely to occur with a RI of 200±100 years, while large to great subduction interface earthquakes of $M_w > 7.5$ to occur every 550±50 years. RI of subduction interface earthquakes suggests alternating periods of intense activity with frequent but smaller earthquakes separated by periods of relative quiescence characterized by rare but more powerful earthquakes.

7. ACKNOWLEDGMENTS

This project was funded by the Centre National de la Recherche Scientifique – Institut National des Sciences de l'Univers (CNRS-INSU Research Program "Aléas, risques et catastrophes telluriques") and the New Zealand Ministry of Science and Innovation (previously Foundation for Research Science and Technology) through their program Paleoseismicity of the Alpine Fault and Hikurangi Margin (C01X0801). This study is part of a PhD undertaken at the Université de Rennes 1 (Géosciences Rennes) and NIWA, funded by a research grant from Ministère de l'Enseignement Supérieur et de la Recherche. The French Ministry of Foreign Affairs (French Embassy in Wellington) and the Université Européenne de Bretagne provided support funds for international travels. Gary Wilson facilitated access to the University of Otago's Geotek Multi-Track Sensor. Alan Orpin, Philip Barnes, Helen Neil, Helen Bostock (NIWA), and Kate Clark and Nichola Litchfield (GNS Science) contributed through numerous constructive discussions. The authors also thank Eulàlia Gràcia (Barcelona Centre for Subsurface Imaging) for her advices on the Oxcal software. Thanks to the two anonymous reviewers for their constructive reviews that helped us to improve the clarity of the paper.

8. REFERENCES

Adams, J., 1990. Paleoseismicity of the Cascadia subduction zone: evidence from turbidites off the Oregon-Washington Margin. Tectonics 9, 569-583.

Addington, L.D., Kuehl, S.A, McNinch, J.E., 2007. Contrasting modes of shelf sediment dispersal off a high-yield river: Waiapu River, New Zealand. Marine Geology 243, 18-30.

Alexander, C.R., Walsh, J.P., Orpin, A.R., 2010. Modern sediment dispersal and accumulation on the outer Poverty continental margin. Marine Geology 270, 213-226.

505 Barnes, P.M., Bostock, H.C., Neil, H.L., Strachan, L.J., Gosling, M., 2013. A 2300-year paleoearthquake
506 record of the southern Alpine Faut and Fiordland subduction zone, New Zealand, based on stacked
507 turbidites. Bulletin of Seismological Society of America 103, 2424-2446, doi: 10.1785/0120120314.

508 Barnes, P.M., Nicol, A., 2004. Formation of an active thrust triangle zone associated with structural
509 inversion in a subduction settings, eastern New Zealand. Tectonics 23, doi: 10.1029/2002TC001449.

510 Barnes, P.M., Nicol, A., Harrison, T., 2002. Late Cenozoic evolution and earthquake potential of an
511 active listric thrust complex above the Hikurangi subduction zone, New Zealand. GSA Bulletin 114,
512 1379-1405.

513 Beavan, J., Tregoning, P., Bevis, M., Kato, T., Meertens, C., 2002. Motion and rigidity of the Pacific
514 Plate and implications for plate boundary deformation. Journal of Geophysical Research, 107, B10,
515 2261, doi:10.1019/2011JB000282.

516 Beck, C., 2009. Late Quaternary lacustrine paleo-seismic archives in north-western Alps: Examples of
517 earthquake-origin assessment of sedimentary disturbances. Earth-Science Reviews 96, 327-344.

518 Berryman, K., 1993. Age, height, and deformation of Holocene marine terraces at Mahia Peninsula,
519 Hikurangi subduction margin, New Zealand. Tectonics 12, 1347-1364.

520 Berryman, K.R., Ota, Y., Hull, A.G., et al., 1989. Holocene paleoseismicity in the fold and thrust belt of
521 the Hikurangi subduction zone, eastern North Island, New Zealand. Tectonophysics 163, 185-195.

522 Blumberg, S., Lamy, F., Arz, H.W., Echtler, H.P., Wiedicke, M., Haug, G.H., Oncken, O., 2008. Turbiditic
523 trench deposits at the South-Chilean active margin: A Pleistocene-Holocene record of climate and
524 tectonics. Earth and Planetary Science Letters 268, 526-539.

525 Bronk-Ramsey, C., 2008. Deposition models for chronological records. Quaternary Science Reviews,
526 27, 42-60.

527 Carter, L., Lamarche, G., Dunkin, M., Mitchell, J., Northcote, L., Wilcox, S., Kuehl, S., Addington, L.,
528 Kniskern, T., Romine, H., Brackley, H., Migeon, S., McNinch, J., Misalis, J., Scione, J., 2003. TAN0314
529 Research Voyage Report, unpublished NIWA Internal report, National Institute of Water and
530 Atmospheric Research, Wellington, New Zealand.

531 Carter, L., Manighetti, B., Ganssen, G., Northcote, L., 2008. Southwest Pacific modulation of abrupt
532 climate change during the Antarctic Cold Reversal – Younger Dryas. Palaeogeography,
533 Palaeaoclimatology, Palaeoecology 260, 284-298.

534 Cochran, U., Berryman, K., Zachariasen, J., Mildenhall, D., Hayward, B., Southall, K., Hollis, C., Barker,
535 P., Wallace, L., Alloway, B., Wilson, K., 2006. Paleoecological insights into subduction zone
536 earthquake occurrence, eastern North Island, New Zealand. Geological Society of America Bulletin
537 118, 1051-1074.

538 Collot, J.Y., Delteil, J., Lewis, K.B., Davy, B., Lamarche, G., Audru, J.C., Barnes, P., Chanier, F.,
539 Chaumillon, E., Lallemand, S., deLepinay, B.M., Orpin, A., Pelletier, B., Sosson, M., Toussaint, B.,
540 Uruski, C., 1996. From oblique subduction to intra-continental transpression: Structures of the
541 southern Kermadec-Hikurangi Margin from multibeam bathymetry, side-scan sonar and seismic
542 reflection. Marine Geophysical Researches 18, 357-381.

543 Collot, J.Y., Lewis, K., Lamarche, G., Lallemand, S., 2001. The giant Ruatoria debris avalanche on the
544 northern Hikurangi Margin, New Zealand: Result of oblique seamount subduction. Journal of
545 Geophysical Research-Solid Earth 106, 19271-19297.

546 Cousins, W.J., Zhao, J.X., Perrin, N.D., et al., 1999. A model for the attenutation of peak ground
547 acceleration in New Zealand earthquakes based on seismograph and accelerograph data. Bulletin of
548 the New Zealand Society for Earthquake Engineering 32, 193-220.

549 Dan, G., Sultan, N., Savoye, B., Deverchere, J., Yelles, K., 2009. Quantifying the role of sandy-silty
550 sediments in generating slope failures during earthquakes: example from the Algerian margin.
551 International Journal of Earth Sciences, 98, 769-789.

552 DeMets, C., Grodon, R. G., Argus, D. F., Stein, S., 1994. Effect of recent revisions to the geomagnetic
553 reversal time scale on estimates of current plate motions. Geophysical Research Letters 21, 2191-
554 2194.

555 Doser, D.I., Webb, T.H., 2003. Source parameters of large historical (1917-1961) earthquakes, North
556 Island, New Zealand. Geophysical Journal International, 152, 795-832.

557 Douglas, J., 2000. A comprehensive worldwide summary of strong-motion attenuation relationships
558 for peak ground acceleration and spectral ordinates (1969 to 2000). Engineering Seismology and
559 Earthquake Engineering Report n°01.1, Imperial College of Science, Technology and Medecine,
560 London, 144p.

561 Downes, G.L., 1995. Atlas of isoseismal maps of New Zealand earthquakes. Institute of Geological and
562 Nuclear Sciences Monograph 11.

563 Downes, G., Webb, T., McSaveney, M., Darby, D., Doser, D., Chagué-Goff, C., Barnett, A., 2000. The
564 March 25 and May 17 1947 Gisborne earthquakes and tsnunamis: implication for tsunami hazard for
565 East Coast, North Island, New Zealand. Tsunami Risk Assessment Beyond 2000, Moscow Tsunami
566 Workshop 2000.

567 Faure, K., Greinert, J., Pecher, I.A., Graham, I.J., Massoth, G.J., De Ronde, C.E.J., Wright, E.T., Olson,
568 E.J., 2006. Methane seepage and its relation to slumping and gas hydrate at the Hikurangi marin,
569 New Zealand. New Zealand Journal of Geology ad Geophysics 49, 503-516.

570 Goff, J., Dominey-Howes, D., 2009. Australasian paleotsunamis – Do Australia and New Zealand have
571 a shared trans-Tasman prehistory? Earth-Science Reviews 97, 147-154.

572 Goldfinger, C., Morey, A.E., Nelson, C.H., Gutierrz-Pastor, J., Johnson, J.E., Karabanov, E., Chaytor, J.,
573 Eriksson, A., Shipboard Scientific Party., 2007. Rutpure lengths and temporal history of significant
574 earthquakes on the offshore and north coast segments of the northern San Andreas Fault based on
575 turbidite stratigraphy. Earth and Planetary Science Letters 254, 9-27.

576 Goldfinger, C., Ikeda, Y., Yeats, R.S., Ren, J., 2013. Superquakes and supercycles. Seismological
577 Research Letters 84, doi: 10.1785/0220110135.

578 Goldfinger, C., Nelson, C.H., Johnson, J.E., Shipboard Sci, P., 2003. Deep-water turbidites as Holocene
579 earthquake proxies: the Cascadia subduction zone and Northern San Andreas Fault systems. Annals
580 of Geophysics 46, 1169-1194.

581 Goldfinger, C., Witter, R.C., Priest, G.R., Wang, K., Zhang, Y.J., Patton, J., Beeson, J. et al., 2009.
582 Cascadia supercycles: Evidence of clustering and Holocene history of energy management from the
583 long Cascadia paleoseismic record. Abstract AGU Chapman Conference on Giant Earthquakes and
584 Their Tsunamis, Chile, May 2010.

585 Goldfinger, C., Nelson, C.H., Morey, A., Johnson, J.E., Gutierrez-Pastor, J., Eriksson, A.T., Karabanov,
586 E., Patton, J., Gracia, E., Enkin, R., Dallimore, A., Dunhill, G., Vallier, T., 2012. Turbidite Event History:
587 Methods and Implications for Holocene Paleoseismicity of the Cascadia Subduction Zone. USGS
588 Professional Paper 1661-F, Reston, VA, U.S. Geological Survey, 184p, 64 Figures.
589 http://pubs.usgs.gov/pp/pp1661f/

590 Gorsline, D.S., De Diego, T., Nava-Sanchez, E.H., 2000. Seismically triggered turbidites in small basins:
591 Alfonso Basin, Western Gulf of California and Santa Monica Basin, California Borderland. Sedimentary
592 Geology 135, 21-35.

593 Gracia, E., Vizcaino, A., Escutia, C., Asioli, A., Rodes, A., Pallas, R., Garcia-Orellana, J., Lebreiro, S.,
594 Goldfinger, C.,. 2010. Holocene earthquake record offshore Portugal (SW Iberia): testing turbidite
595 paleoseismology in a slow-convergent margin. Quaternary Science Reviews 29, 1156-1172.

596 Hicks, D.M., Gomez, B., Trustrum, N.A., 2004. Event suspended sediment characteristics and the
597 generation of hyperpycnal plumes at river mouths: East Coast Continental Margin, North Island, New
598 Zealand. Journal of Geology 112, 471-485.

599 Hicks, D.M., Shankar, U., 2003. Sediment yield from New Zealand rivers. NIWA chart, Miscellaneous
600 series N.79. National Institute of Water and Atmospheric Research, Wellington, New Zealand.

601 Higham, T.F.G., Hogg, A.G., 1995. Radiocarbon dating of prehistoric shell from New Zealand and
602 calculation of the Delta R value using fish otoliths. Radiocarbon 37, 409-416.

603 Huh, C.A., Su, C.C., Liang., W.T., Ling, C.Y., 2004. Linkages between turbidites in the southern
604 Okinawa Trough and submarine earthquakes. Geophysical Research Letters, 31, L12304,
605 doi:10/1029/2004GL019731.

606 Joanne, C., Collot, J.Y., Lamarche, G., Migeon, S., 2010. Continental slope reconstruction after a giant
607 mass failure, the example of the Matakaoa Margin, New Zealand. Marine Geology 268, 67-84.

608 Kalish, J.M., 1993. Pre-bomb and post-bomb radiocarbon in fish ololiths. Earth and Planetary Science
609 Letters 114, 549-554.

610 Kettner, A.J., Gomez, B., Syvitski, J.P.M., 2007. Modeling suspended sediment discharge from the
611 Waipaoa River system, New Zealand: The last 3000 years. Water Resources Research 43.

612 Kniskern, T.A., Kuehl, S.A., Harris, C.K., Carter, L., 2010. Sediment accumulation patterns and fine-
613 scale strata formation on the Waiapu River shelf, New Zealand. Marine Geology 270, 188-201.

614 Lamarche, G., Joanne, C., Collot, J.Y., 2008a. Successive, large mass-transport deposits in the south
615 Kermadec fore-arc basin, New Zealand: The Matakaoa submarine instability complex. Geochemistry
616 Geophysics Geosystems 9, Q04001, doi:10.1029/2007GC001843.

617 Lamarche, G., Orpin, A., Wilcox, S., Verdier, A.-L., Amyes, D., Woelz, S., McGill, K., 2008b. R.V.
618 Tangaraoa TAN0810 Voyage Report: Transfer of extensional deformation, submarine instabilities and
619 paleoearthquake proxy, unpublished NIWA Internal report N°135, National Institute of Water and
620 Atmospheric Research, Wellington, New Zealand.

621 Lee, H.J., Edwards, B.D., 1986. Regional assess offshore slope stability. Journal of Geotechnical
622 Engineering-ASCE 112, 489-509.

623 Lee, H.J., Locat, J., Dartnell, P., Israel, K., Wong, F. et al., 1999. Regional variability of slope stability:
624 application to the Eel margin, California. Marine Geology 154, 305-321.

625 Lewis, K.B., 1973. Ashes, turbidites, and rates of sedimentation on the continental slope off Hawke
626 Bay. New Zealand Journal of Geology and Geophysics 16, 439-454.

627 Lewis, K.B., 1980. Quaternary sedimentation on the Hikurangi oblique-subduction and transform
628 margin, New Zealand. In: Sedimentation in oblique slip mobile zone. Balance, P.F., Reading, H.G.
629 (Eds). Special Publication International Association of Sedimentologists 4, 171-189.

630 Lewis, K.B., Marshall, B.A., 1996. Seep faunas and other indicators of methane-rich dewatering on
631 New Zealand convergent margins. New Zealand Journal of Geology ad Geophysics 39, 181-200.

632 Lewis, K.B., Lallemand, S.E., Carter, L., 2004. Collapse in a Quaternary shelf basin off East Cape, New
633 Zealand: evidence for passage of a subducted seamount inboard of the Ruatoria giant avalanche.
634 New Zealand Journal of Geology ad Geophysics 47, 415-429.

635 Lewis, K.B., Pettinga, J.R., 1993. The merging, imbricate frontal wedge of the Hikurangi Margin. In:
636 Balance, P.F. (Ed.), South Pacific Sedimentary Basins. Sedimentary Basins of the World, vol. 2. Elsevier
637 Science Publishers, Amsterdam, pp. 225-250.

638 Litchfield, N.J.; Van Dissen, R.; Sutherland, R.; Barnes, P.M.; Cox, S.C.; Norris, R.; Beavan, J.; Langridge,
639 R.M.; Villamor, P.; Berryman, K.R.; Stirling, M.W.; Nicol, A.; Nodder, S.D.; Lamarche, G.; Barrell, D.J.A.;
640 Pettinga, J.R.; Little, T.; Pondard, N.; Mountjoy, J. and Clark, K.J. (in press). A model of active faulting
641 in New Zealand. New Zealand Journal of Geology and Geophysics.

642 Litchfield, N., Wilson, K., Berryman, K., Wallace, L., 2010. Coastal uplift mechanisms at Pakarae River
643 mouth: Constraints from a combined Holocene fluvial and marine terrace dataset. Marine Geology
644 270, 72-83.

645 Lowe, D.J., Shane, P.A.R., Alloway, B.V., Newnham, R.M., 2008. Fingerprints and age models for
646 widespread New Zealand tephra marker beds erupted since 30,000 years ago: a framework for NZ-
647 INTIMATE. Quaternary Science Reviews 27, 95-126.

648 Lykousis, V., Roussakis, R., Alexandri, M., Pavlakis, P., Papoulia, I., et al., 2002. Sliding and regional
649 slope stability in active margins: North Aegean Trough (Mediterranean). Marine Geology 186, 281-
650 298.

651 Ma, Y., Friedrichs, C.T., Harris, C.K., Donelson Wright, L., 2010. Deposition by seasonal wave- and
652 current-supported sediment gravity flows interacting with spatially varying bathymetry : Waiapu
653 shelf, New Zealand. Marine Geology 275, 199-211.

654 McGlone, M.S., Wilmshurst, J.M. 1999. Dating initial Maori environmental impacts in New Zealand.
655 Quaternary International 59, 5-16.

656 McHugh, C.M., Seeber, L., Braudy, N., Cormier, M.H., Davis, M.B., Diebold, J.B., Dieudonne, N.,
657 Douilly, R., Gulick, S.P.S., Hornbach, M.J., Johnson III, H.E., Ryan Miskin, K., Sorlien, C.C., Steckler,
658 M.S., Symithe, S.J., Templeton, J et al., 20101. Offshore sedimentary effects of the 12 January 2010
659 Haiti earthquake. Geology 39, 723-726.

660 Mountjoy, J.J., Micallef, A., 2011. Polyphase emplacement of a 30 km3 blocky debris avalanche and
661 its role in slope-gully development. In: Submarine Mass Movements and Their Consequences,
662 Advances in Natural and Technological Hazards Research 31, doi:10/1007/978-94-007-2162-3_19.

663 Mulder, T., Weber, O., Anschutz, P., Jorissen, F.J., Jouanneau, J.M., 2001. A few months-old storm-
664 generated turbidite deposited in the Capbreton Canyon (Bay of Biscay, SW France). Geo-Marine
665 Letters 21, 149-156.

666 Nakajima, T., Kanai, Y., 2000. Sedimentary features of seismoturbidites triggered by the 1983 and
667 older historical earthquakes in the eastern margin of the Japan Sea. Sedimentary Geology 135, 1-19.

668 Nicol, A., and Wallace, L.M., 2007. Temporal stability of deformation rates: comparison of geological
669 and geodetic observations, Hikurangi subduction margin, New Zealand. Earth and Planetary Science
670 Letters 258, 397-413.

671 Noda, A., TuZino, T., Kanai, Y., Furukawa, R., Uchida, J.I., 2008. Paleoseismicity along the southern
672 Kuril Trench deduced from submarine-fan turbidites. Marine Geology 254, 73-90.

673 Orpin, A.R., 2004. Holocene sediment deposition on the Poverty-slope margin by the muddy
674 Waipaoa River, East Coast New Zealand. Marine Geology 209, 69-90.

675 Orpin, A.R., Alexander, C., Carter, L., Kuehl, S., Walsh, J.P., 2006. Temporal and spatial complexity in
676 post-glacial sedimentation on the tectonically active, Poverty Bay continental margin of New
677 Zealand. Continental Shelf Research 26, 2205-2224.

678 Page., M.J., Trustum, N.A., Orpin, A.R., Carter, L., Gomez, B., Cochran, U.A., Mildenhall, D.C., Rogers,
679 K.M., Brackley, H.L., Palmer, A.S., Northcote, L., 2010. Storm frequency and magnitude in response to
680 Holocene climate variability, Lake Tutira, North-Eastern New Zealand. Marine Geology 270, 30-44.

681 Paquet, F., Proust, J.N., Barnes, P.M., Pettinga, J.R., 2009. Inner-forearc sequence architecture in
682 response to climatic and tectonic forcing since 150 ka: Hawke's Bay, New Zealand. Journal of
683 Sedimentary Research 79, 97-124.

684 Paquet, F., Proust, J.N., Barnes, P.M., Pettinga, J.R., 2011. Controls on active forearc basin
685 stratigraphy and sediment fluxes: The Pleistocene of Hawke Bay, New Zealand. GSA Bulletin 123,
686 1074-1096.

687 Patton, J.R., Goldfinger, C., Morey, A.E., Romsos, C., Black, B., Djadjadihardja, Y., Udrekh, 2013.
688 Seismoturbidite record as preserved at core sites at the Cascadia and Sumatra-Andaman subduction
689 zones. Natural Hazards and Earth System Sciences 13, 833-867.

690 Patton, J., Goldfinger, C., Morey, A.E., Djadjadihardja, Y., Hanifa, U, 201009. Temporal clustering,
691 energy-state proxy, and recurrence of Holocene paleo-earthquakes in the region of the 2004
692 Sumatra-Andaman earthquake. Abstract AGU Chapman Conference on Giant Earthquakes and Their
693 Tsunamis, Chile, May 2010.

694 Pedley, K.L., Barnes, P.M., Pettinga, J.R., Lewis, K.B., 2010. Seafloor structural geomorphic evolution
695 of the accretionary frontal wedge in response to seamount subduction, Poverty Indentation, New
696 Zealand. Marine Geology 270, 119-138.

697 Pouderoux, H., 2012. Gravity flow sedimentation and paleoseismicity of an active margin: the
698 example of the Hikurangi subduction margin of New Zealand. Published Ph.D. thesis. Mémoire de
699 Géosciences Rennes 142, 347p.

700 Pouderoux, H., Proust, J.N., Lamarche, G., Orpin, A., Neil, H., 2012a. Deep-sea sedimentation along
701 the Hikurangi subduction margin (New Zealand) since the Last Glacial Maximum: characterisation,
702 timing and origin of turbidites. Marine Geology, 295-298, 51-76.

703 Pouderoux, H., Lamarche, G., Proust, J-N., 2012b. Building a 18 000-year-long paleo-earthquake
704 record from detailed deep-sea turbidite characterisation in Poverty Bay, New Zealand. Natural
705 Hazards and Earth System Sciences 12, 1-25.

706 Power, W., Wallace, L., Wang, X., Reyners, M et al., 2011. Tsunami hazard posed to New Zealand by
707 the Kermadec and southern New Hybrides subduction margins: an assessment based on plate
708 boundary kinematics, interseismic coupling, and historical seismicity. Pure and Applied Geophysics,
709 doi:10.1007/s00024-011-0299-x.

710 Proust, J-N., Lamarche, G., Migeon, S., Neil, H., and Shipboard Party, 2006. MD152/MATACORE
711 Tectonic and climate controls on sediment budget. Les rapports de campagnes à la mer, Institut Paul
712 Emile Victor, 107p.

713 Proust, J.N., Lamarche G., Migeon, S., Neil, H.L., 2008. Climate and tectonic changes in the ocean
714 around New Zealand. EOS Transaction American Geophysical Union 89, 277-288.

715 Puig, P., Ogston, A.S., Mullenbach, B.L., Nittrouer, C.A., Parsons, J.D., Sternberg, R.W., 2004. Storm-
716 induced sediment gravity flows at the head of the Eel submarine canyon, northern California margin.
717 Journal of Geophysical Research-Oceans 109.

718 Reyners, M., McGinty, P., 1999. Shallow subduction tectonics in the Raukumara peninsula, New
719 Zealand, as illuminated by earthquake focal mechanisms. Journal of Geophysical Research-Solid Earth
720 104, 3025-3034.

721 Reyners, M., 1993, Lateral segmentation of the subducted plate at the Hikurangi Margin, New
722 Zealand: seismological evidence: Tectonophysics, v. 96, p. 203-223.

723 Reyners, M., 1998, Plate coupling and the hazard of large subduction thrust earthquakes at the
724 Hikurangi subduction zone, New Zealand: New Zealand Journal of Geology and Geophysics, v. 41, p.
725 343-354.

726 Shane, P., 2000. Tephrochronology: a New Zealand case study. Earth Science Reviews 49, 223-259.

727 Shanmugam, G., 2006. The Tsunamite problem. Journal of Sedimentary Research 76, 718-730.

728 Si, H., Midorikwawka, S., 1999. New attenuation relations for peak ground acceleration and velocity
729 considering effects of fault type and site conditions. Proceeding of 12th World Conference on
730 Earthquake Engineering. Translated in English in 2000. Journal of Structural and Construction
731 Engineering, (Transaction of Architectural Institute of Japan) 523, 63-70.

732 Sikes, E.L., Samson, C.R., Guilderson, T.P., Howard, W.R., 2000. Old radiocarbon ages in the
733 southwest Pacific Ocean during the last glacial period and deglaciation. Nature 405, 555-559.

734 St-Onge, G., Mulder, T., Piper, D.J.W., Hillaire-Marcel, C., Stoner, J.S., 2004. Earthquake and flood-
735 induced turbidites in the Saguenay Fjord (Quebec): a Holocene paleoseismicity record. Quaternary
736 Science Reviews 23, 283-294.

737 Stirling, M., McVerry, G., Gerstenberger, M., Litchfield, N., Van Dissen, R., Berryman, K., Barnes, P.,
738 Wallace, L., Bradley, B., Villamor, P., Langridge, R., Lamarche, G., Nodder, S., Reyners, M., Bradley, B.,
739 Rhoades, D., Smith, W., Nicol, A., Pettinga, J., Clark, K. and Jacobs, K., 2012. National Seismic Hazard
740 Model for New Zealand: 2010 Update. Bulletin of the Seismological Society of America 102, 1514-
741 1542.

742 Stirling, M., Rhoades, D., Berryman, K., 2002. Comparison of earthquake scaling relations derived
743 from data of the instrumental and preinstrumental era. Bulletin of the Seismological Society of
744 America 92, 812-830.

745 Strasser, M., Anselmetti, F.S., Fäh, D., Giardini, D., Schnellmann, M., 2006. Magnitudes and source
746 areas of large prehistoric northern Alpine earthquakes revealed by slope failures in lakes. Geology 34,
747 1005-1008, doi: 10.1130/G22784.A1.

748 Strasser, M., Stegmann, S., Bussmann, F., Anselmetti, F.S., Rick, B., Kopf, A., 2007. Quantifying
749 subaqueous slope stability during seismic shaking: Lake Lucerne as model for ocean margins. Marine
750 Geology 240, 77-97.

751 Wallace, L.M., Reyners, M., Cochran, U., Bannister, S., Barnes, P.M., Berryman, K., Downes, G.,
752 Eberhart-Phillips, D., Fagereng, A., Ellis, S., Nicol, A., McCaffrey, R., Beavan, R.J., Henrys, S.,
753 Sutherland, R., Barker, D.H.N., Litchfield, N., Townend, J., Robinson, R., Bell, R., Wilson, K., Power, W.,
754 2009. Characterizing the seismogenic zone of a major plate boundary subduction thrust: Hikurangi
755 Margin, New Zealand. Geochemistry Geophysics Geosystems 10, Q100006.

756 Wallace, L.M.J., Beavan, J., McCaffrey, R., Darby, D. et al., 2004. Subduction zone coupling and
757 tectonic block rotations in the North Island, New Zealand. Journal of Geophysical Research 109,
758 B12406, doi:10.1029/2004JB003241.

759 Webb, T.H., Anderson, H., 1998. Focal mechanisms of large earthquakes in the North Island of New
760 Zealand: slip partitioning at an oblique active margin. Geophysical Journal International 134, 40-86.

761 Wiesner, M.G., Wang, Y., Zheng, L., 1995. Fallout of volcanic ash to the deep South China Sea induced
762 by the 1991 eruption of Mount Pinatubo (Philippines). Geology 23, 885-888.

763 Wilson, K., Berryman, K., Cochran, U., Little, T., 2007. Early Holocene paleoseismic history at the
764 Pakarae locality, eastern North Island, New Zealand, inferred from transgressive marine sequence
765 architecture. Tectonics 26, TC4013, 18pp.

766 Wilson, K., Berryman, K., Litchfield, N., Little, T., 2006. A revision of mid-late Holocene marine terrace
767 distribution and chronology at the Pakarae River mouth, North Island, New Zealand. New Zealand
768 Journal of Geology and Geophysics 49, 477-489.
769

9. FIGURE CAPTIONS

Figure 1 - Morpho-tectonic settings of the northern Hikurangi Margin, New Zealand. Red dots show sediment cores used in this study. The present day average sediment deliveries of the three main rivers, which catchments are highlighted in grey shade, are indicated in dark grey (from Hicks and Shankar et al., 2003). White squares are locations of coastal paleo-earthquakes evidences in (A) Pakarae river mouth, (B) Mahia Peninsula, and (C) northern Hawke's Bay. Bold lines indicate the main earthquake sources identified by Stirling et al. (2012) and Litchfield et al. (in press) (see also SM1 Table SM1). Bold teeth-line indicates the subduction front. Insert: the Kermadec-Hikurangi margin with the Pacific (PAC) and the Australian (AUS) plates, the Wairarapa (W), Hawke Bay (HB) and Raukumara (R) regions, and the Central Volcanic Region (CVR). Dark arrow is relative plate motion at the plate boundary from Beavan et al. (2002).

Figure 2 - Characterisation of turbidites and hemipelagite from visual (photo), internal structures (X Ray), Geotek petrophysical properties (gamma density, magnetic susceptibility and P-wave velocity) and grain size (sand, silt and clay percentage). Peaks in grain size correspond to peaks in the Geotek; the turbidites' fining up trend is illustrated by the Geotek measurements.

Figure 3 - Example of the Oxcal age model from a giant piston core (MD06-3009) and two short piston cores (Tan0810-2 and -6), showing the sedimentation rate of hemipelagite through time. The *k* parameter is used to define the regularity of the sedimentation rate along the core: the higher the *k* parameter, the more linear the sedimentation rate and the smaller the turbidite age uncertainties. Since hemipelagite settles at an assumed roughly constant rate, the highest *k* parameter was chosen for each core. All ages are plotted with their 2σ age range.

Figure 4 - Simplified correlation diagram of turbidites between cores in Ruatoria (upper slope, Ruatoria Debris Avalanche and Hikurangi Trough). Detailed correlations in SM2 Fig. SM2.01. Dashed lines are tephra. Basin events are labelled Rx. The c. 6 ka boundary (thin black line) is the average basal boundary of short cores. Black stars on isolated events show events correlated to basin events in Poverty and indicated unrecognised basin events in Ruatoria (see text for details). Number on the left of logs are turbidite facies as in Table 1.

Figure 5 - Simplified correlation diagram of turbidites between cores in Matakaoa (channel and levees in the turbidite plain and fan). Detailed correlations in SM2 Fig. SM2.02. Cores are arranged upstream to downstream from left to right; see caption and legend in figure 4.

Figure 6 - Example of margin-scale correlation of turbidites using one core from Poverty, two from Ruatoria and two from Matakaoa. Each re-entrant is c. 100 km apart. Detailed correlations in SM2 Fig. SM2.03. Turbidites are indicated by basic core log, facies (number from 1 to 5) and Geotek petrophysical properties (density and magnetic susceptibility). See legend and caption in figure 4. Margin events are labelled Hx. The age of tephra layers (purple) is reported in cal. yr BP.

Figure 7 - Temporal correlation between margin events and onland evidences of paleo-earthquakes from the Pakarae river mouth (A; Wilson et al., 2006; 2007), Mahia Peninsula (B; Berryman et al., 1993), and northern Hawke's Bay (C; Cochran et al., 2006), and paleo-tsunamis identified along the east coast of the North Island East Coast (Goff and Dominey-Howes, 2009). Purple bands are age range of correlated margin events. Large margin events interpreted as the record of subduction interface earthquakes are framed in red.

Figure 8 - Examples of isomagnitude maps defining the area shaken by an earthquake of a given magnitude, which can trigger synchronous slope failures in the source areas of the turbidites (blue area in the upper slope). Grey dots show the location of sediment cores. Each map is generated from an empirical relationship that defines the Peak Ground Acceleration (PGA) from the magnitude, depth, distance and type of earthquakes (see SM3 for details). Faults capable of producing earthquake shaking large enough to generate turbidity currents in the source area are shown in bold red (epicentre shown by red dots) and summarized in Table 5. Blue dots are epicentres of earthquakes that cannot generated ground-shaking capable of generating turbidites in the source area. In each map, the isomagnitude M_w 7.5 is shown as an example of the methodology used to define the Mw 7.5 area. (A) Isomagnitude map built from the relationship of Cousins et al. (1999), labelled Eq. (1). PGA = 0.08g is reached simultaneously in the upper slope of Poverty and Ruatoria for a $M_w \geq 6.5$ earthquake located between both re-entrants. This corresponds to the activity of only two upper plate faults (red bold lines). See SM3 Fig. SM3 for subduction interface earthquakes isomagnitude maps. (B) Isomagnitude map built from the relationship of Si and Midoriwaka (1999), labelled Eq. (2). PGA = 0.1 g is reached simultaneously in the three re-entrants for $M_w \geq 7.2$ earthquakes located between Poverty and Ruatoria. This corresponds to the rupture of the subduction interface. No upper plate faults can trigger synchronous slope failures in the three re-entrants.

Figure 9 - Recurrence intervals (RI) of large paleo-earthquakes at the origin of margin events *vs* time. (A) RI of $M_w \geq 7.3$ earthquakes at the origin of the 41 margin events identified over the last c. 16.5 kyr (grey line). Dots correspond to the average age of the margin event H*x* *vs* the average time span since the last one. The recurrence intervals of $M_w > 7.5$ earthquake at the origin of the 20 large margin events is indicated by dashed blue line. (B) Distribution of RI of $M_w > 7.5$ earthquakes showing an alternation of active periods in light yellow with low RI and numerous earthquakes, and quiescence periods in light blue during which larger RI are noted (for each period, average RI are noted in italic and their duration noted in bold).

Figure 10 - Frequency diagrams of paleo-earthquakes during (A) the Late Holocene and (B) the Late Pleistocene – Early Holocene. The latter is likely to be underestimated due to uncertainties discussed in the paper. $M_w > 7.5$ earthquakes correspond to large margin events and $M_w \geq 7.3$ earthquakes to all margin events (see text for details). Histograms (grey bars) show the frequency of recurrence interval (RI) within each bin of 100 years, with their statistical distribution estimated for each centile (black line). The median RI of each plot is noted in white for histograms and in black for the statistical distribution (cross).

10. TABLES

Table 1 – Lithotype characteristics of deep-sea sediments along the northern Hikurangi Margin (summarized from Pouderoux et al., 2012a).

Table 2 – Location and characteristics of sediment cores used in this study. T: gravity flow deposits (turbidites); H: hemipelagite.

Table 3 – Range of petrophysical properties of hemipelagite and turbidites calculated from the cores.

Table 4 – Margin events (Hx) modelled age deduced from basin events correlation in Poverty, Ruatoria and Matakaoa.

857 **Table 5** – Earthquake sources and estimated magnitude deduced from the overlap of isomagnitude
858 maps (Fig. 8; see also SM3 Fig. SM3) and the known active faults complied by Stirling et al (2012).
859 Different scenarios are considered according tothe two type of margin events, the three PGA
860 thresholds for slope failures triggering and the two empirical relationships used to build
861 isomagnitude maps .

862

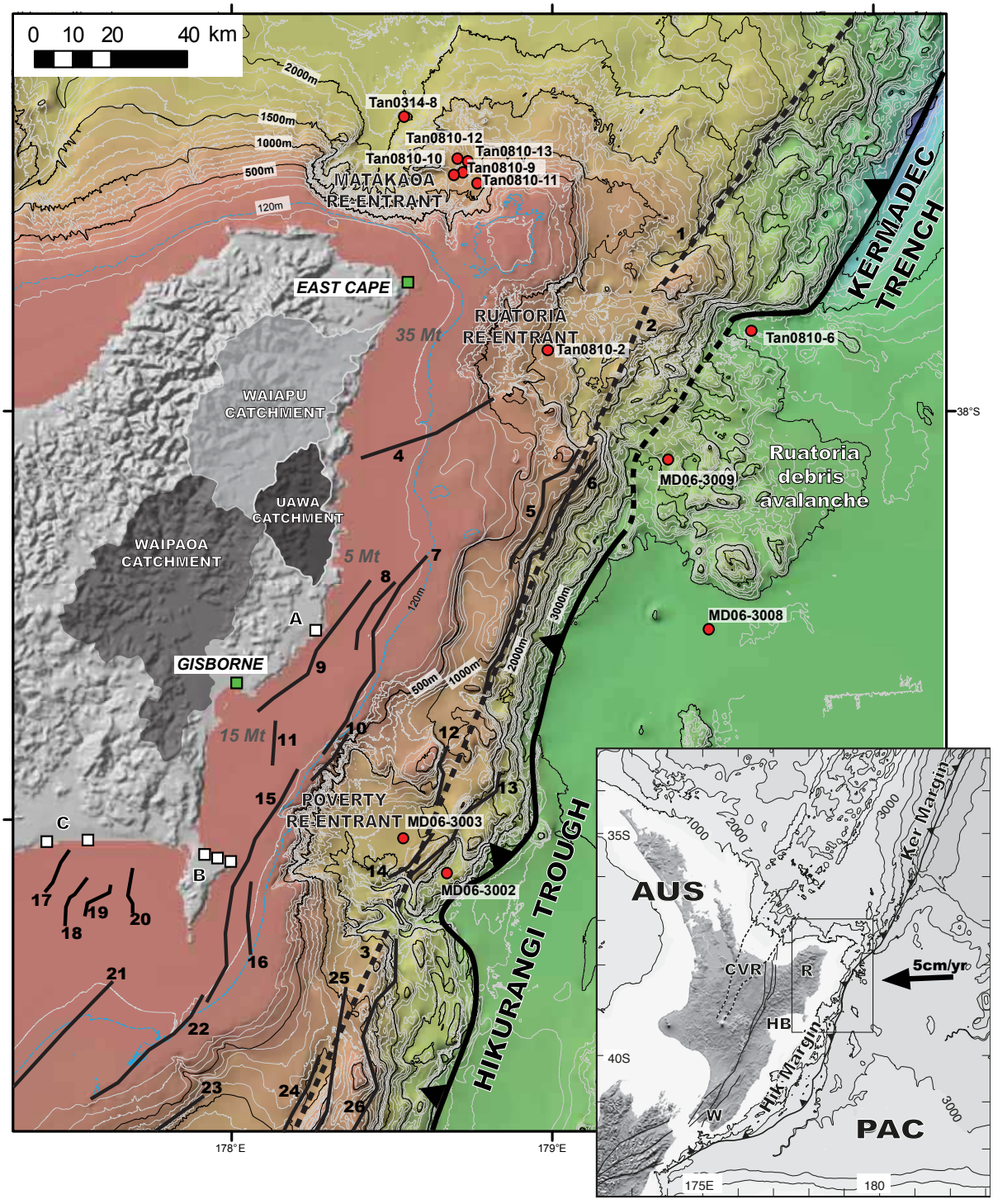
0 10 20 40 km
2000m
1500m
1000m
500m
120m
Tan0314-8
Tan0810-12
Tan0810-13
Tan0810-10
Tan0810-9
Tan0810-11
MATAKAOA RE-ENTRANT
EAST CAPE
35 Mt
RUATORIA RE-ENTRANT
Tan0810-2
Tan0810-6
KERMADEC TRENCH
WAIAPU CATCHMENT
UAWA CATCHMENT
WAIPAOA CATCHMENT
5 Mt
15 Mt
GISBORNE
MD06-3009
Ruatoria debris avalanche
MD06-3008
3000m
2000m
1000m
500m
POVERTY RE-ENTRANT
MD06-3003
MD06-3002
HIKURANGI TROUGH
38°S
178°E
179°E
A
B
C
1
2
3
4
5
6
7
8
9
10
11
12
13
14
15
16
17
18
19
20
21
22
23
24
25
26
35S
40S
AUS
PAC
CVR
R
HB
W
5cm/yr
Ker Margin
Hik Margin
1000
2000
3000
175E
180

Figure 1

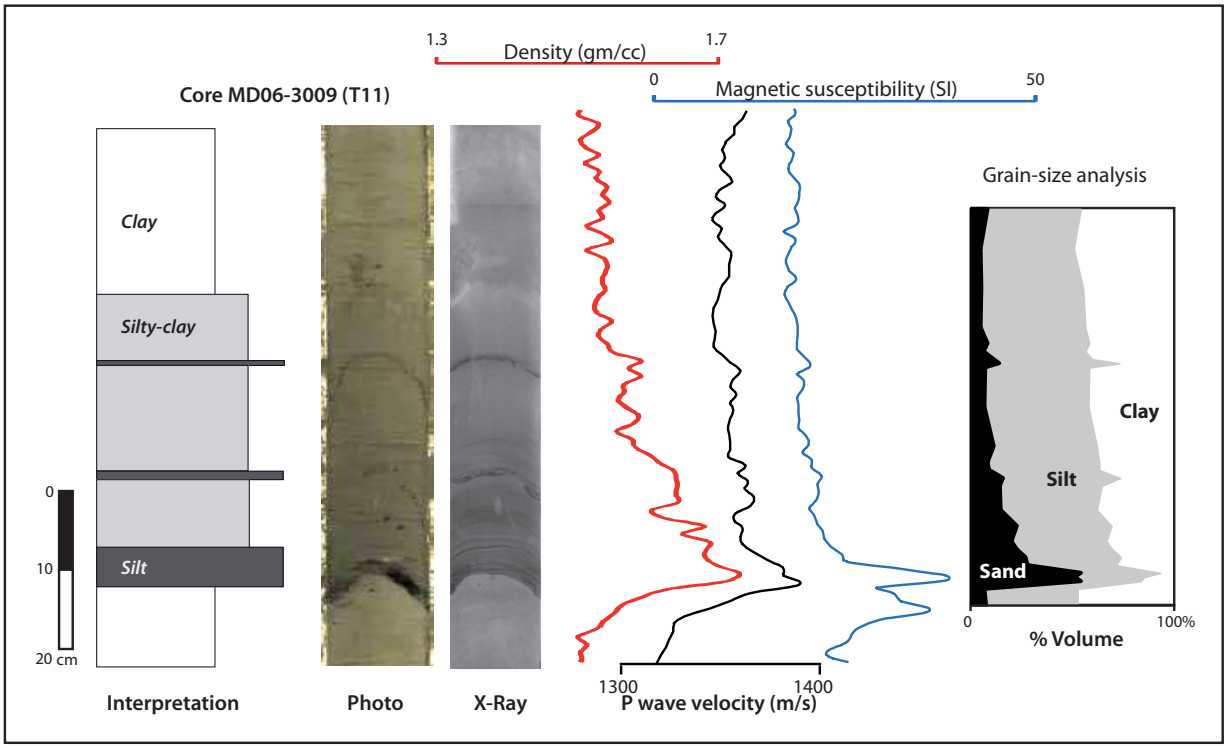
1.3
Density (gm/cc)
1.7
0
Magnetic susceptibility (SI)
50
Core MD06-3009 (T11)
Grain-size analysis
Clay
Silty-clay
Silt
0
10
20 cm
Clay
Silt
Sand
0
100%
% Volume
Interpretation
Photo
X-Ray
1300
1400
P wave velocity (m/s)

Figure 2

Figure 3

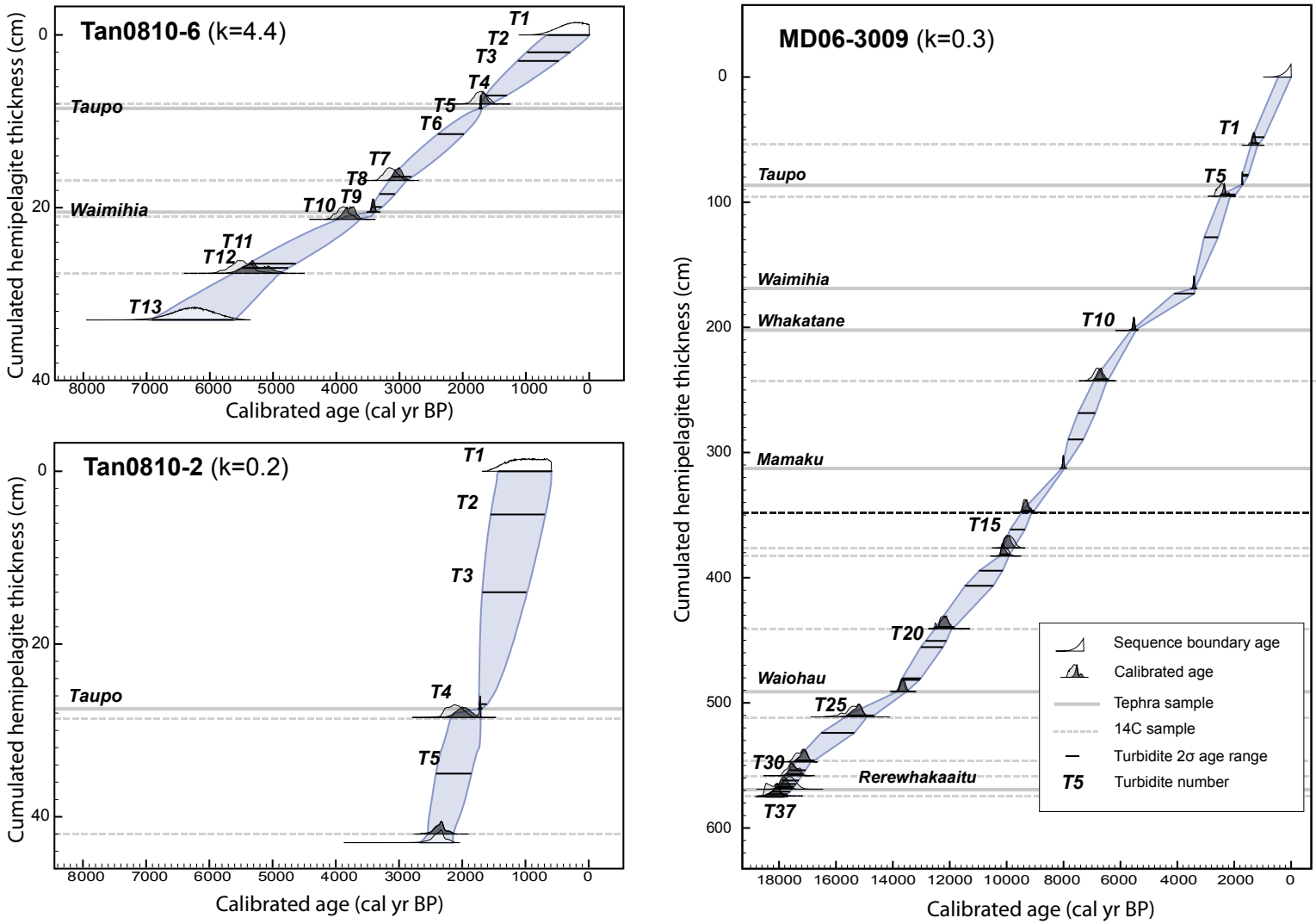
Tan0810-6 (k=4.4)
Cumulated hemipelagite thickness (cm)
Calibrated age (cal yr BP)
Taupo
Waimihia
T1
T2
T3
T4
T5
T6
T7
T8
T9
T10
T11
T12
T13
Tan0810-2 (k=0.2)
MD06-3009 (k=0.3)
Whakatane
Mamaku
Waiohau
Rerewhakaaitu
T15
T20
T25
T30
T37
Sequence boundary age
Calibrated age
Tephra sample
14C sample
Turbidite 2σ age range
Turbidite number

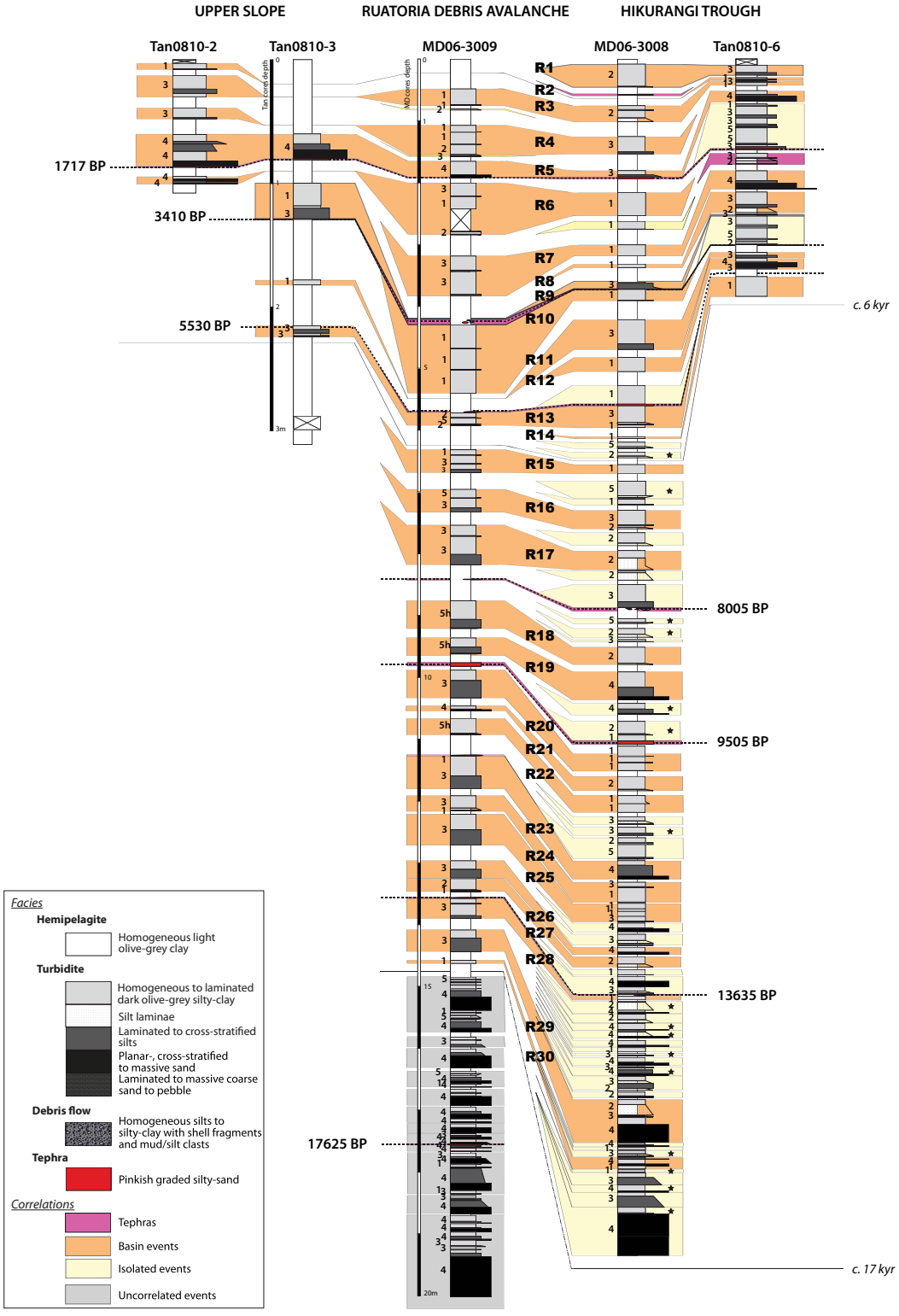
UPPER SLOPE
RUATORIA DEBRIS AVALANCHE
HIKURANGI TROUGH
Tan0810-2
Tan0810-3
MD06-3009
MD06-3008
Tan0810-6
1717 BP
3410 BP
5530 BP
8005 BP
9505 BP
13635 BP
17625 BP
c. 6 kyr
c. 17 kyr
R1
R2
R3
R4
R5
R6
R7
R8
R9
R10
R11
R12
R13
R14
R15
R16
R17
R18
R19
R20
R21
R22
R23
R24
R25
R26
R27
R28
R29
R30
Facies
Hemipelagite
Homogeneous light olive-grey clay
Turbidite
Homogeneous to laminated dark olive-grey silty-clay
Silt laminae
Laminated to cross-stratified silts
Planar-, cross-stratified to massive sand
Laminated to massive coarse sand to pebble
Debris flow
Homogeneous silts to silty-clay with shell fragments and mud/silt clasts
Tephra
Pinkish graded silty-sand
Correlations
Tephras
Basin events
Isolated events
Uncorrelated events

Figure 4

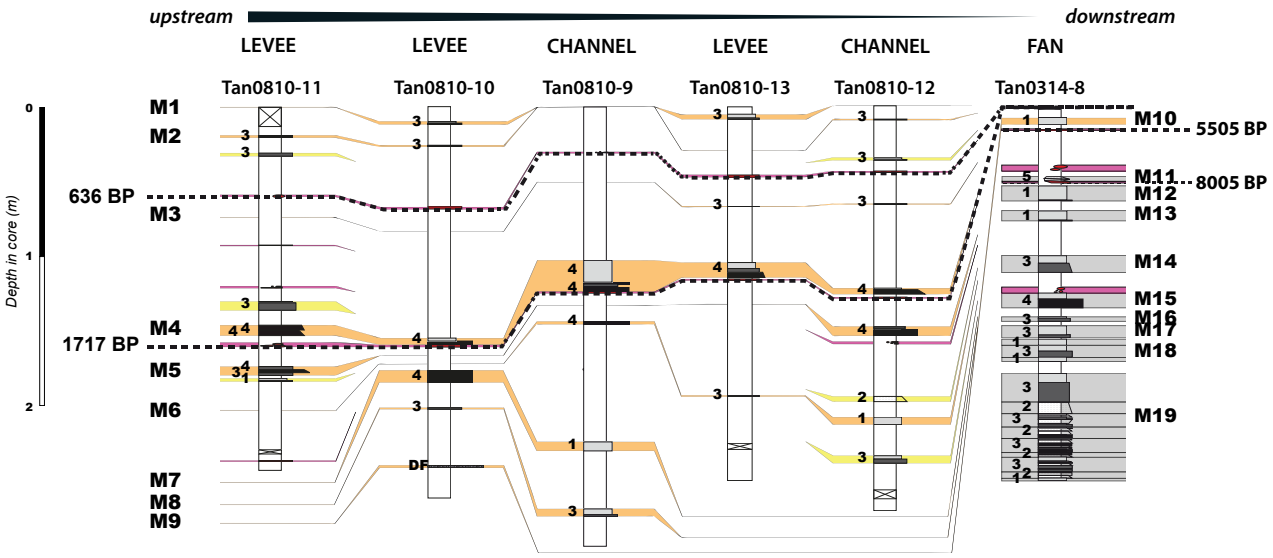
upstream
downstream
LEVEE
LEVEE
CHANNEL
LEVEE
CHANNEL
FAN
Tan0810-11
Tan0810-10
Tan0810-9
Tan0810-13
Tan0810-12
Tan0314-8
Depth in core (m)
0
1
2
M1
M2
636 BP
M3
M4
1717 BP
M5
M6
M7
M8
M9
M10
5505 BP
M11
8005 BP
M12
M13
M14
M15
M16
M17
M18
M19
DF

Figure 5

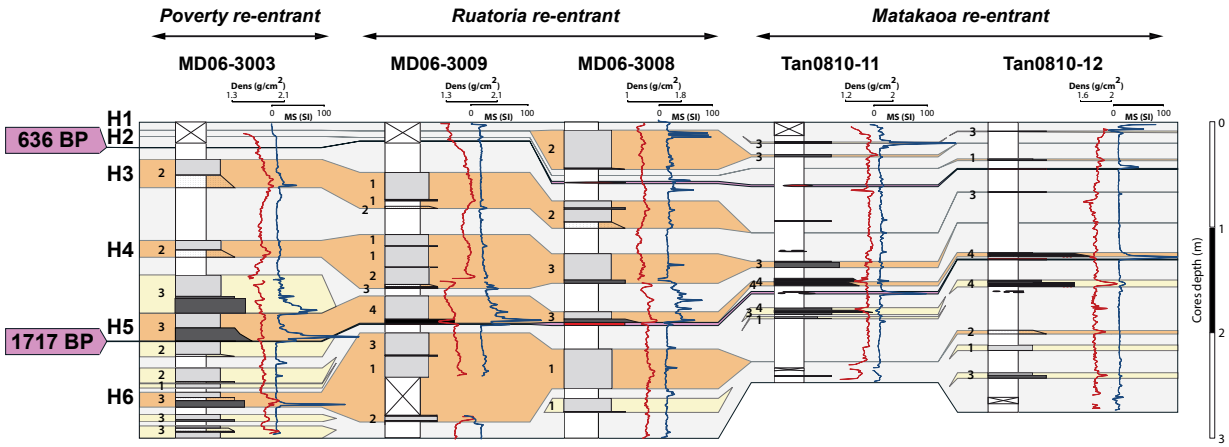
Poverty re-entrant
Ruatoria re-entrant
Matakaoa re-entrant
MD06-3003
MD06-3009
MD06-3008
Tan0810-11
Tan0810-12
Dens (g/cm3)
MS (SI)
636 BP
1717 BP
H1
H2
H3
H4
H5
H6
Cores depth (m)

Figure 6

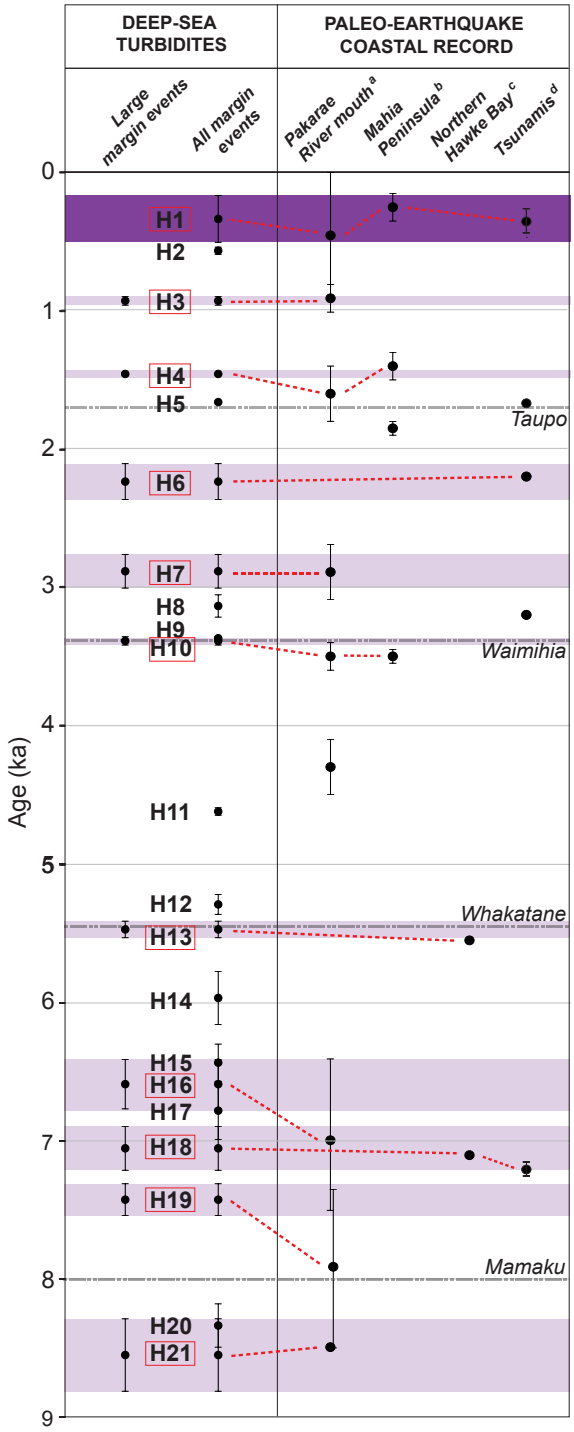
DEEP-SEA TURBIDITES
PALEO-EARTHQUAKE COASTAL RECORD
Large margin events
All margin events
Pakarae River mouth a
Mahia Peninsula b
Northern Hawke Bay c
Tsunamis d
Age (ka)
0
1
2
3
4
5
6
7
8
9
H1
H2
H3
H4
H5
H6
H7
H8
H9
H10
H11
H12
H13
H14
H15
H16
H17
H18
H19
H20
H21
Taupo
Waimihia
Whakatane
Mamaku

Figure 7

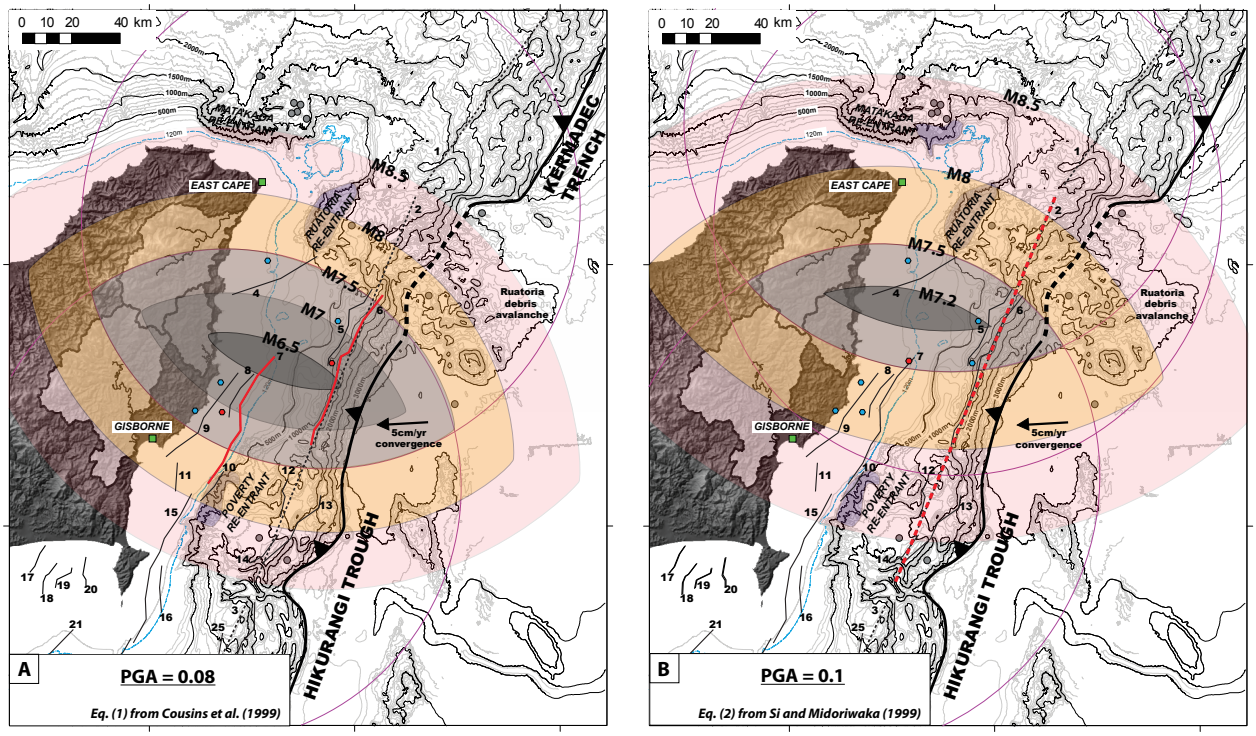
0 10 20 40 km
MATAKAOA RE-ENTRANT
EAST CAPE
KERMADEC TRENCH
M8.5
RUATORIA RE-ENTRANT
M8
M7.5
M7
M6.5
Ruatoria debris avalanche
GISBORNE
5cm/yr convergence
POVERTY RE-ENTRANT
HIKURANGI TROUGH
A
PGA = 0.08
Eq. (1) from Cousins et al. (1999)
0 10 20 40 km
MATAKAOA RE-ENTRANT
EAST CAPE
M8.5
M8
M7.5
M7.2
RUATORIA RE-ENTRANT
Ruatoria debris avalanche
GISBORNE
5cm/yr convergence
POVERTY RE-ENTRANT
HIKURANGI TROUGH
B
PGA = 0.1
Eq. (2) from Si and Midoriwaka (1999)

Figure 8

A - Recurrence interval of earthquakes
at the origin of all margin events (n=41)

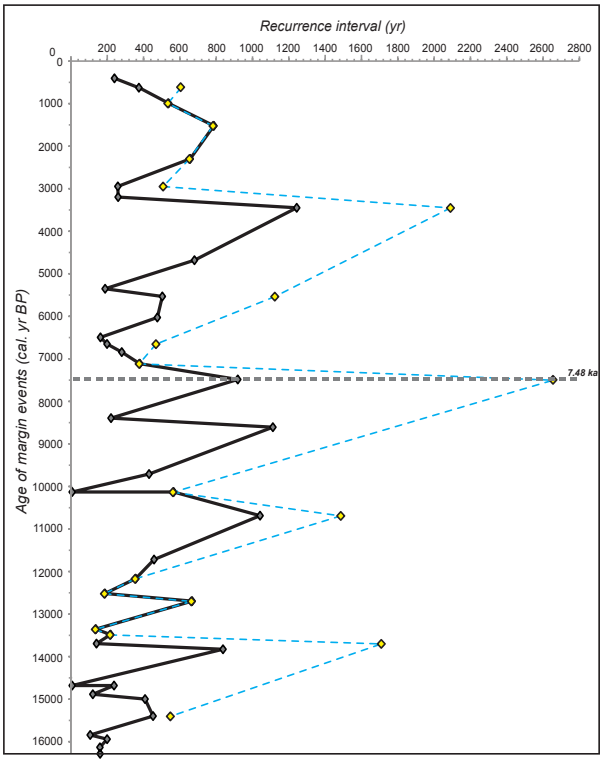

B - Recurrence interval of earthquakes
at the origin of largemargin events (n=20)

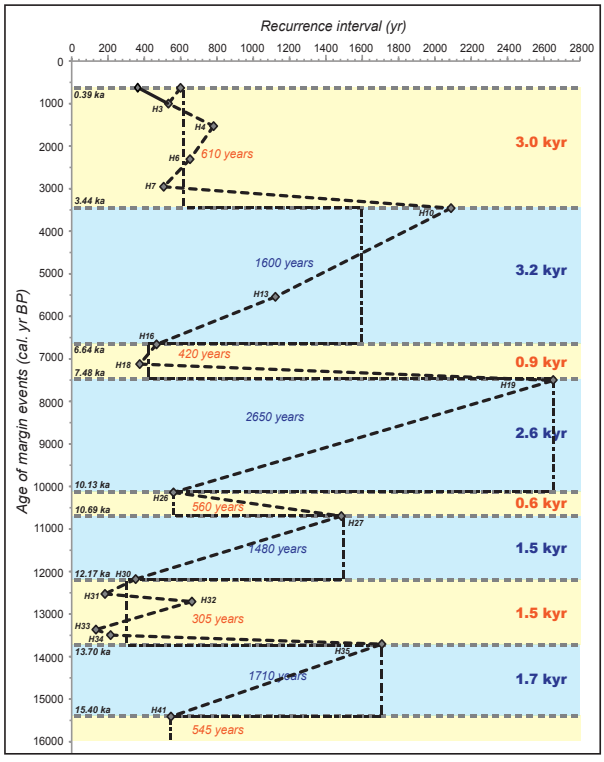

Figure 9

A - Recurrence interval of earthquakes during the Late Holocene

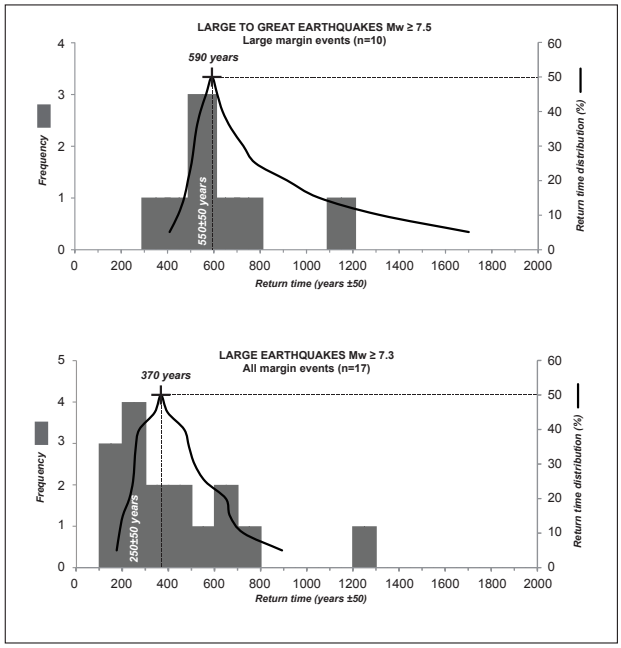

B - Recurrence interval of earthquakes during the Late Pleistocene - Early Holocene

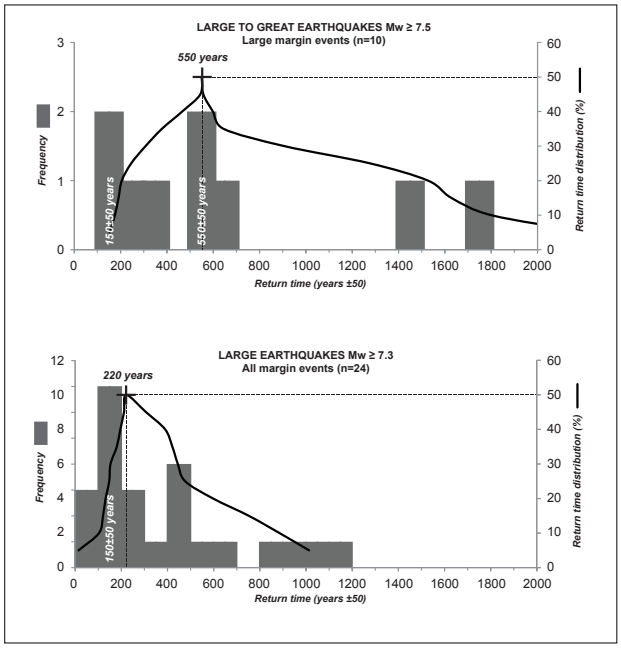

Figure 10

Lithotype	Texture	Colour	Grain size (microns)	Thickness (cm)	Composition (sand fraction)	Depositional process
Hemipelagite	Homogenised, heavily bioturbated silty-clay	Olive-grey	<10	0.5-> 50 cm	Volcaniclastic grains,quartz, planktonic organisms	Marine sedimentation
Tephra	Graded silts	Pinkish	10-20	<10 cm	Volcaniclastic debris (glass shards and pumiceous lapilli)	Airfall volcanic ash
Debrite	Chaotic silty-clay with sand to pebble size particules or deformed stratified lithoclasts	Dark olive-grey	*NA*	<35 cm	Quartz, volcaniclastic debris, bivalve and gasteropod shells, clasts of laminated silty-clays	Debris flow
Turbidite	Sandy to silty base grading up to silty-clay	Dark olive-grey	10-> 200	0.5-75 cm	Volcaniclastic debris, light minerals, rock fragments, foraminifers, shell fragments	Turbidity current
1 Muddy turbidite	*Thin silt lamina overlain by massive silty-clay*	*Dark olive-grey*	*10-20*	*1-40 cm*	*Quartz, foraminifers*	*Very low density turbidity current*
2 Silt laminae turbidite	*Interbedded, thinning and fining up clay and silt laminae*	*Dark olive-grey*	*10-20*	*1-40 cm*	*Quartz, volcanoclastic debris*	*Low density turbidity current*
3 Silty turbidites	*Fining upward clayey silt sequence*	*Dark olive-grey*	*10-< 100*	*0.5-55 cm*	*Volcaniclastic debris, quartz, foraminifers, micas*	*low to medium density turbidity current*
4 Sandy turbidites	*Sand base grading up to silty-clay*	*Dark olive-grey*	*10-> 100*	*1-75 cm*	*Quartz, volcaniclastic debris, rock fragments, micas, heavy minerals*	*Medium density turbidity current*
5 Hyperpcynite	*Basal reverse graded turbidite*	*Olive-grey*	*10-< 100*	*5-45 cm*	*Foraminifers, wood fragments, quartz, volcaniclastic debris*	*Hyperpcynal flow*

Table 1

Core	Longitude		Latitude		Water depth (m)	Core length (m) *	Composition		Number of gravity-flow deposits	Thickness of gravity-flow deposits (cm)			
	deg.	min.	deg.	min.			T	H		Min	Max	Mean	*s.d.*
MD 06-3002	39	7.83	178	40.31	2305	*20 (12)*	75%	25%	100	1.5	22	7.6	*4.4*
MD 06-3003	39	2.79	178	32.17	1398	*12.88*	77%	23%	101	1	36	9.8	*6.8*
MD 06-3008	38	32.12	179	32.04	3520	*25.4 (19)*	75%	25%	89	2	48	16	*10.8*
MD 06-3009	38	7.02	177	21.69	2940	*20*	70%	30%	77	1	76	17.9	*14.9*
TAN0810-2	37	50.973	178	59.201	1078	*1.65*	60%	40%	8	2	18	8	*4.8*
TAN0810-3	37	52.691	178	57.289	1090	*3.2*	22%	78%	6	3	20	10.3	*6.6*
TAN0810-6	37	48.105	179	37.228	3400	*1.8*	82%	18%	25	1	18.5	6.1	*4.1*
TAN0314-8	37	16.088	178	32.29	2034	*2.51*	63%	37%	20	2	11.5	7	*2.9*
TAN0810-9	37	24.5876	178	43.108	1180	*3.2*	12%	88%	5	2	16	6.8	*4.8*
TAN0810-10	37	24.77	178	41.799	1159	*2.2*	8%	92%	6	1	8	3	*2.5*
TAN0810-11	37	26.1094	178	45.8894	1089	*2.6*	12%	88%	8	1.5	6	3.1	*1.4*
TAN0810-12	37	23.382	178	42.851	1255	*2.75*	11%	89%	8	0.5	6	3.3	*2*
TAN0810-13	37	23.55	178	44.054	1167	*2.5*	7%	93%	4	1	10	3.9	*3.7*

**: full recovered length; when core deformation is too high, the used core length is given between brackets.*
***: total number of turbidite layers identified in the core.*

Table 2

Re-entrant	Core	Core depth (m)	Gamma density (g/cm2)		Magnetic susceptibility (SI)		P-Wave velocity (m/s)	
			H	T	H	T	H	T
Ruatoria	*MD06-3009*	*2940*	1.4 - 1.6	1.4 - 2	10 - 25	15 - 100	1300 - 1500	1350 - 1700
	MD06-3008	*3520*	1.1 - 1.4	1.2-1.7	10 - 25	15 - 100	1650 - 1700	1775 - 1950
	Tan0810-6	*3400*	1.7 - 1.8	1.7 - 2	10 - 25	15 - 100	1650 - 1700	1700 - 1800
Matakaoa	*Tan0810-10 to -*	*1168±82*	1.6 - 1.8	1.6 - 2	10	10 - 100	1225 - 1425	1400 - 1550
	Tan0314-8	*2034*	1.8	1.8 - 2.1	15	15 - 50	1225	1225 - 1375
Poverty	*MD06-3003*	*1398*	1.8	1.8 - 2.2	10	10 - 100	1300	1300 - 1500
	MD06-3002	*2305*	1.8	1.8 - 2.2	60	60 - 120	1400	1400 - 1600

H: hemipelgite; T: turbidites

Table 3

Table 4

MARGIN EVENTS			Poverty re-entrant					Ruatoria re-entrant							Matakaoa re-entrant								
	EVENT			EVENT		CORE			EVENT		CORE						EVENT		CORE					
name	mean age	2σ range	name	mean age	2σ range	MD3003	MD3002	name	mean age	2σ range	Tan0810-2	Tan0810-3	MD06-3009	MD06-3008	Tan0810-6	name	mean age	2σ range	Tan0810-9	Tan0810-10	Tan0810-11	Tan0810-12	Tan0810-13	Tan0314-8
H1	**387**	**170**						**R1**	387	253				T1	T1		*387*	*170*			*T2*			
H2	**616**	**26**						**R2**	789	199	T1				T2		*529*	*114*				*T2*		
H3	**978**	**32**	**P1**	819	*191*	T1		**R3**	1040	94	T2		T1	T2	T3	**M3**	941	212				T3	T3	
H4	**1508**	**13**	**P2**	1388	*132*	T2		**R4**	1566	71	T3		T3	T3			*1499*	*188*			*T3*			
H5 **	**1711**	**6**	**P3**	1699	*38*	T3		**R5**	1711	6	T4	T1	T5	T4	T4	**M4**	1716	11	T1	T3	T4	T4	T3	
H6	**2286**	**130**	**P7**	2426	*270*	T6		**R6**	2185	232	T5		T6	T5			*2255*	*245*				*T6*		
H7	**2935**	**122**	**P9**	2880	*212*	T8		**R7**	2935	122			T7	T7	T7									
H8	**3186**	**81**	**P11**	3060	*206*	T10		**R8**	3201	125				T8	T8	**M7**	3657	552	T3	T4				
H9 **	**3419**	**11**	**P13**	3438	*30*	T12		**R9**	3391	39		T2		T9	T9									
H10	**3438**	**30**	**P14**	3438	*30*	T12		**R10**	3462	69			T8	T9										
H11	**4672**	**27**	**P17**	4357	*342*	T15		**R11**	4821	176		T3		T10	T11									
H12	**5344**	**72**	**P18**	5409	*137*	T16		**R12**	5132	326				T11	T12	**M9**	5127	289		T6				T1
H13	**5525**	**60**	**P19**	5535	*77*	T17		**R13**	5525	60		T4	T9-10	T12										
H14	**6021**	**193**	**P23**	6021	*193*	T22	T1	**R14**	6072	445				T13	T13									
H15	**6489**	**135**	**P24**	6489	*135*	T23	T2		*6303*	*583*				*T15*										
H16	**6644**	**179**	**P25**	6644	*179*	T24	T3	**R15**	6668	248			T11	T16										
H17	**6836**	**210**	**P26**	6836	*210*	T25	T4		*6926*	*311*				*T17*										
H18	**7108**	**159**	**P27**	7039	*228*	T26	T5	**R16**	7221	272			T12	T19										
H19	**7480**	**116**	**P28**	7480	*116*	T27	T8	**R17**	7570	269			T13	T21										
H20	**8390**	**157**	**P30**	8390	*157*	T29	T19		*8624*	*612*				*T24*										
H21	**8603**	**262**	**P33**	8604	*263*	T32	T22		*8800*	*654*				*T25*										
H22 *	**9128**	**101**	**P34**	9067	*161*	T33	T24	**R18**	9240	213			T14	T27										
H23 *	**9505**	**25**	**P37**	9505	*25*	T36	T27	**R19**	9617	260			T15	T28		**M12**	9325	750						T4
H24	**9706**	**143**	**P38**	9706	*143*	T37	T28		*9839*	*393*				*T29*										
H25	**10129**	**103**	**P40**	10155	*129*	T39	T31		*10010*	*221*				*T30*										
H26	**10129**	**103**	**P42**	10169	*143*	T39	T32	**R20**	10073	159			T16	T31										
H27	**10686**	**113**	**P45**	10579	*220*	T40	T35	**R21**	10767	194			T17	T32										
H28 *	**11340**	**118**	**P48**	11532	*310*	T41	T39	**R22**	11256	201			T18	T33										
H29	**11719**	**289**	**P49**	11659	*348*	T42	T40		*11896*	*466*				*T35*										
H30	**12169**	**291**	**P50**	12081	*378*	T43	T42	**R23**	12189	311			T19	T37		**M13**	12290	970						T5
H31	**12518**	**242**	**P51**	12518	*242*	T44	T43	**R24**	12481	365			T20	T38										
H32	**12698**	**264**	**P52**	12698	*264*	T45	T44	**R25**	12628	391			T21	T40										
H33	**13357**	**238**	**P54**	13357	*238*	T48	T46	**R26**	13348	330			T22	T42		**M14**	13564	814						T6
H34	**13487**	**210**	**P55**	13490	*213*	T49	T47	**R27**	13377	320			T23	T43										
H35	**13698**	**143**	**P56**	13736	*181*	T50	T53	**R28**	13678	162			T24	T47		**M15**	14338	594						T7
H36	**13831**	**187**	**P57**	13831	*187*	T51	T54		*14233*	*717*				*T48*										
H37	**14661**	**271**	**P58**	14685	*295*	T56	T55		*14299*	*783*				*T49*										
H38	**14661**	**271**	**P59**	14685	*295*	T56	T56		*14365*	*823*				*T50*										
H39	**14890**	**295**	**P60**	14890	*295*	T58	T57		*14728*	*901*				*T53*										
H40	**15004**	**307**	**P61**	14993	*317*	T60	T58		*15163*	*466*				*T55*										
H41	**15404**	**224**	**P62**	15549	*369*	T62	T59	**R29**	15350	278			T25	T58		**M17**	15016	698						T9
H42	**15849**	**388**	**P63**	15849	*388*	T63	T60		*15865*	*653*				*T61*										
H43	**15983**	**357**	**P64**	15948	*393*	T64	T60	**R30**	15935	583			T26	T62		**M18**	16404	778						T10
H44	**16140**	**398**	**P65**	16140	*398*	T65	T60		*16050*	*698*				*T63*										
H45	**16292**	**295**	**P66**	16292	*295*	T66	T61		*16056*	*704*				*T64*										
H46	**16446**	**314**	**P66**	16451	*319*	T67	T62		*16056*	*704*				*T64*										

**, ** are margin events related to catastrophic floods or volcanism (after Pouderoux et al., 2012a)*
Isolated events are in italic grey

All margin events (n=41)

	Cousins et al. (1999) - Eq. (1)			*Si and Midoriwaka (1999) - Eq. (2)*		
PGA	**Faults ***	**RI ****	**Mw range**	**Faults ***	**RI ****	**Mw range**
0.08	2; 6; 7	390-460 years	7.3-8.4	2; 6; 7	390-460 years	7.3-8.4
0.1	2; 6	890-1235 years	7.3-8.4	2; 6; 7	390-460 years	7.3-8.4
0.15	2	1300-1670 years	8.2-8.4	2	1300-1670 years	8.2-8.4

**: Numbers correspond to faults detailed in Table SM1; ** Recurrence intervals calculated for the duration of our turbidite record (16,060 years, from 390 to 16,450 yr BP)*
Average recurrence interval deduced from the turbidite record : 400 years

Large margin events (n=20)

	Cousins et al. (1999) - Eq. (1)			*Si and Midoriwaka (1999) - Eq. (2)*		
PGA	**Faults ***	**RI ****	**Mw range**	**Faults ***	**RI ****	**Mw range**
0.08	2	1300-1670 years	8.2-8.4	2; 6	890-1235 years	7.3-8.4
0.1	ø	ø	ø	2	1300-1670 years	8.2-8.4
0.15	ø	ø	ø	2	1300-1670 years	8.2-8.4

**: Numbers correspond to faults detailed in Table SM; ** Recurrence intervals calculated for the duration of our turbidite record (16,060 years, from 390 to 16,450 yr BP)*
Average recurrence interval deduced from the turbidite record : 800 years

Table 5